Critical Parameters Influencing Mixed CH_4/CO_2 Hydrates Dissociation during Multistep Depressurization

Ouyang, Qian; Shanker Pandey, Jyoti; von Solms, Nicolas

Published in:
Fuel

Link to article, DOI:
10.1016/j.fuel.2022.123985

Publication date:
2022

Document Version
Publisher's PDF, also known as Version of record

Fuel 320 (2022) 123985

Contents lists available at ScienceDirect

Fuel

journal homepage: www.elsevier.com/locate/fuel

Full Length Article

Critical parameters influencing mixed CH_4/CO_2 hydrates dissociation during multistep depressurization

Qian Ouyang, Jyoti Shanker Pandey *, Nicolas von Solms *

Center for Energy Resource Engineering (CERE), Department of Chemical Engineering, Technical University of Denmark, 2800 Kgs. Lyngby, Denmark

ARTICLE INFO

Keywords:
Natural gas hydrate
Multistep depressurization
CH_4 recovery
CO_2 storage
Resistance

ABSTRACT

Early studies show that multistep depressurization of CH_4/CO_2 mixed hydrates generates additional CH_4 while storing CO_2 in hydrate-bearing sediments. There are many critical factors that could affect the production and storage efficiency of this method. However, it is unclear how to achieve high efficiency in both CH_4 production and CO_2 storage by controlling these critical parameters. In this experimental work, we identified three critical parameters (CH_4/CO_2 ratio in mixed hydrates, residual water saturation (S_{rw}), and shut-in period) and investigated their effects on production parameters (CH_4 molar fraction in the gas phase (XCH_4), CH_4 recovery percentage (RCH_4), and CO_2 storage ratio (SCO_2)). Experiments were performed on sandstone cores using a high-pressure core flooding system equipped with pressure, temperature, and electrical resistivity measurements. Gas composition was analyzed by gas chromatography. The results showed that the optimal production parameters were determined at low S_{rw} of 43.7–47.4% and higher CH_4/CO_2 ratio of 1.76–2.06 in CH_4/CO_2 mixed hydrates. The optimized values were obtained at the equilibrium pressure of CH_4/CO_2 hydrate system at a specific reservoir temperature without water production during pressure release. In addition, the period between two pressure releases had a direct effect on the production and storage performances, and the most efficient production and storage was measured at 4-hour shut-in period of pressure release. The measured percent changes in normalized resistivity (ΔNR_2) were dependent on S_{rw} and shut-in period. Positive increase of ΔNR_2 indicated increased hydrate saturation or improved water gas distribution in the sediment during multistep depressurization. The results demonstrated the importance of three critical parameters in designing an effective production and storage scheme after CO_2 injection into CH_4 hydrates.

1. Introduction

Natural gas hydrates (NGHs) are solid-crystalline compounds consisting of host water molecules and gas molecules (CH_4, C_2H_6, CO_2 and H_2). Cage-like structures are formed by hydrogen-bonded water with gas molecules stabilizing inside under low temperature and high pressure [1]. NGHs are widely recognized as promising clean hydrocarbon energy for abundant reserves in marine sediments (0–110 m below seabed) and permafrost regions (130–500 m below underground) [2,3]. The total amount of global hydrate-bonded CH_4 reserve is reported to be within the scale of 10^{15}-10^{18} standard cubic meters (ST m^3), exceeding the known amount of conventional oil and gas resources [4–6]. Furthermore, noted that CH_4 is a kind of high-density energy with the combustion heat of approximately 890 kJ/mol and therefore regarded as one of the most excellent alternative energy sources in the 21st century [7]. Due to the vast reserve and high energy density of NGHs, an increasing number of researches have been conducted on NGHs exploitation in recent years.

Exploitation methods refer to those that recover natural gas (the majority are CH_4) from NGHs within reservoir, which mainly include depressurization [8,9], thermal stimulation [10,11], inhibitor injection [12,13] and CH_4-CO_2 swapping [14,15]. The depressurization method reduces the reservoir pressure, thus drawing thermodynamic conditions out of the hydrate stability zone. This thermodynamic instability causes NGHs to decompose and produce CH_4 and water. However, endothermic dissociation of NGHs via rapid pressure drop can cause partial ice or hydrate reformation and then stop CH_4 production. Thermal stimulation is also a thermodynamic method that disrupts phase equilibrium conditions of NGHs. However, large heat loss makes it uneconomical, and more effective heating techniques need to be investigated. Inhibitor injection can moderate the equilibrium of NGHs and thus inducing hydrate dissociation. However, this exploitation method is restricted in

* Corresponding authors.
E-mail addresses: jyshp@kt.dtu.dk (J.S. Pandey), nvs@kt.dtu.dk (N. von Solms).

https://doi.org/10.1016/j.fuel.2022.123985
Received 18 November 2021; Received in revised form 2 March 2022; Accepted 24 March 2022
Available online 30 March 2022

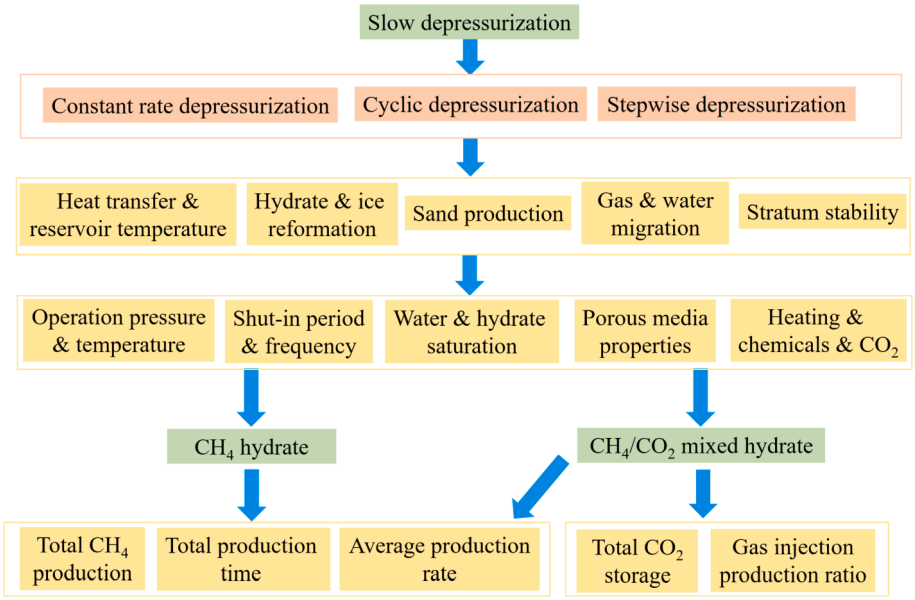

Fig. 1. Slow depressurization-based method for hydrate exploitation from CH_4 hydrate and CH_4/CO_2 mixed hydrate with its technical concerns, affecting factors, and efficiency parameters.

application because of high cost and environmental pollution. Compared to other methods, CH_4-CO_2 swapping is an energy efficient and non-hazardous method, and can achieve a win-win situation of simultaneous CH_4 recovery and CO_2 sequestration [16,17]. The principle is that CO_2 can form hydrate under more moderate thermodynamic conditions, replacing CH_4 in existing hydrate cages by forming new CO_2 hydrates [18]. This kind of swapping process between CH_4 and CO_2 without violent destruction of the hydrate structure can stabilize the stratum that probably collapses during the NGH exploitation process through depressurization and thermal stimulation [19].

Among these exploitation methods, depressurization is demonstrated to be the most commercial method and has been used to develop NGHs in several field tests [20–23]. Rapid/direct depressurization technique tends to trigger the formation of ice or secondary hydrates, which blocks fluid flow channels and reduces gas production. To avoid these problematic issues, a slow depressurization technique with well-controlled pressure drop rate or gradient pressure drop was designed, achieving efficient and continuous gas production. Fig. 1 presents an overview of slow depressurization-based CH_4 production from CH_4 hydrate and CH_4/CO_2 mixed hydrate together with its technical concerns, which affect factors and efficiency parameters. As shown in Fig. 1, this technique can be mainly classified into constant-rate depressurization [24,25], cyclic depressurization [26,27] and stepwise depressurization [28–30]. These well-controlled slow depressurization may simultaneously reduce water production through gas/water migration and avoid stratum instability without sand production. The key parameters that affect gas production efficiencies include operating factors (depressurization pressure/temperature and shut-in period/frequency) and properties of the in situ reservoir (water/hydrate saturation and porous media) [31]. Another aspect that affects slow depressurization-based gas production is to combine it with other exploitation methods, such as depressurization combined with thermal stimulation/heating, with chemical inhibitor injection, and with CO_2 gas injection.

The single CH_4-CO_2 swapping method cannot meet the commercial NGH exploitation requirements due to the low CH_4 gas recovery efficiency [32]. The main reason for this low gas production is mass transfer caused by the formation of CO_2 hydrate films around CH_4 hydrates [33–35]. And the hydrate films also reduce gas molecules transport and CO_2 concentration around the surface of CH_4 hydrate by decreasing relative gas permeability. To overcome the drawbacks of CH_4-CO_2 swapping, the combination of swapping with the methods mentioned above have been studied [36–38], one of which is CH_4-CO_2 swapping combined with depressurization. This kind of combination method has been proven to be effective in the production testing of the Inik Sikumi field, where CO_2-rich gas injection and depressurization were performed accordingly, with a total of 24,410 STm^3 CH_4 recovered from the hydrate-containing reservoir during a whole production period of 30 days [39]. The exploitation patterns of CH_4-CO_2 swapping combined with depressurization have also been reported in many experimental investigations. Zhao et al. revealed that CH_4-CO_2 swapping could be divided into two stages, and depressurization could induce partial melting of CH_4 hydrates and create pathways for CO_2 penetration in the second stage [36]. Chen et al. verified the feasibility of enhancing CH_4 recovery and CO_2 storage simultaneously with the assistance of depressurization operation. These two evaluation parameters of performance were integrated and indicated by the single parameter of CO_2 utilization efficiency. The results showed that both outlet and inlet pressures greatly affected CO_2 efficiency [40]. Yang et al. investigated flue gas injection into gas hydrate reservoir with further depressurization to generate CH_4-rich gas (up to 90 mol%) while storing CO_2 efficiently into hydrate (up to 80 mol%) [41,42]. In another study, Heydari and Peyvandi performed CH_4-CO_2 swapping followed by pressure reduction with the addition of rhamnolipid. The result of the CH_4 mole fraction was around 52 mol% in the gas phase, with the CH_4 recovery efficiency of 18.02% at the ending point [43]. These studies, however, paid less attention to the simultaneous maximization of CH_4 recovery and CO_2 storage. To do this, strategies can be decided from thermodynamic consideration. Goel [44] proved that the partial pressure of CH_4 increased with the decomposition of CH_4 hydrates, and a small amount of the decomposed CH_4 gas could reform hydrates when the partial pressure of CH_4 reached the phase equilibrium of the mixed CH_4/CO_2 hydrates. Nevertheless, the ideal operation pressure is that between the equilibrium of CH_4 hydrates and CO_2 hydrates to release as much as CH_4 while storing as much as CO_2 from the perspective of thermodynamic stability [45,46].

It is known that hydrate loss would increase pore pressure and weaken soil particles link, triggering instability of sediments. CH_4-CO_2 swapping can address this concern by storing CO_2 in the form of hydrates, and CO_2 hydrate-bearing sediments are stiffer than CH_4 hydrate-bearing sediments [47]. It is anticipated that further depressurization on

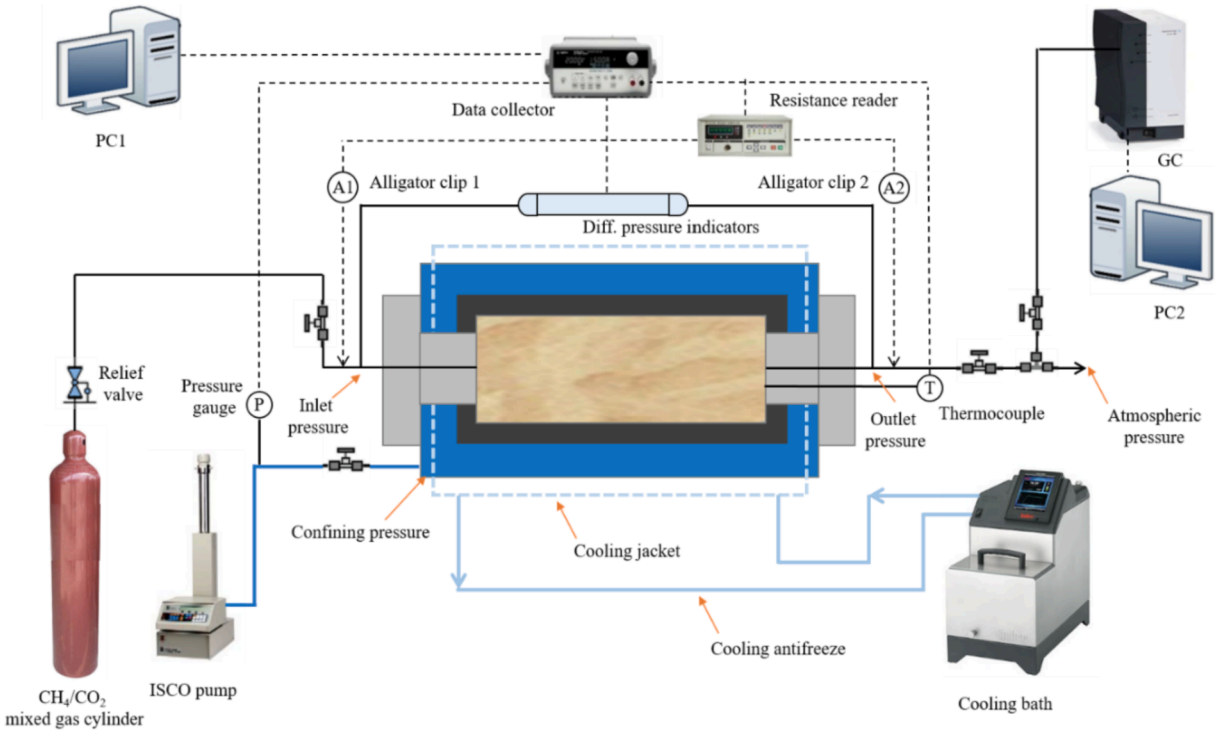

Fig. 2. Schematic of the experimental setup of CH_4/CO_2 mixed hydrate formation and exploitation.

hydrates sample would cause a redistribution of CH_4/CO_2 in hydrate and change of hydrate volume accordingly. Thus, it is needed to quantify the volume change of CH_4/CO_2 hydrates to consider potential stiffness failure of hydrate-bearing sediments because too much hydrate loss may loosen cementation or skeleton of sediment [48]. From the perspective of electrical properties, NGHs are electric insulator and electrical resistance as one of the crucial electrical properties, can represent hydrate saturation in hydrate-bearing sediment system. It is proved that electrical resistance increased with hydrate formation and decreased with hydrate decomposition [49,50]. And it could be more reasonable to evaluate whether the stability of hydrate-bearing sediment was improved or not by electrical resistivity instead of hydrate volume change, because electrical resistivity was mainly affected by fluid saturation, types of guest molecules and total hydrate volume [51]. Although the study showed that pure CO_2 hydrates have lower resistance than pure CH_4 hydrates [52], the resistivity behavior of CH_4-rich and CO_2-rich mixed hydrates during depressurization is still not well understood.

In our preliminary investigation, depressurization combined with CH_4-CO_2 swapping was designed, i.e. replacing the residual CH_4 within the hydrate cage with CO_2 after the operation of pressure reduction [33]. However, water production and hydrate reformation problems occurred when employing this combination method to exploit NGHs, though CH_4 recovery efficiency was enhanced. In another experimental study, CH_4-CO_2 swapping combined with three-stage gradient depressurization was proposed to address the problem of mass transfer during CH_4-CO_2 swapping exploitation of NGHs [53]. According to the phase equilibrium difference between CH_4 hydrates and CO_2 hydrates, depressurization after CH_4-CO_2 swapping would enhance CH_4 production and CO_2 storage within a hydrate-bearing reservoir at the pressure below equilibrium conditions for CH_4 hydrates as well as above that for CO_2 hydrates. This assumption has been demonstrated by our recent studies, in which CH_4/CO_2 mixed hydrates dissociation induced by controlled multistep depressurization can increase both CH_4 recovery and CO_2 storage more efficiently [45,46,54]. However, different influencing factors on CH_4 recovery and CO_2 storage performance have not been comprehensively analyzed thus far. More importantly, unknowns on the optimization of both CH_4 recovery and CO_2 storage still exist.

Fig. 3. Picture of sandstone sample and rubber sleeve.

This study extended investigation on CH_4-CO_2 swapping combined with depressurization by experimentally studying CH_4/CO_2 mixed hydrate dissociation through controlled multistep depressurization. Assumptions were preset that CH_4-CO_2 swapping for NGHs exploitation has already occurred and CH_4/CO_2 mixed hydrate have formed before multistep depressurization. Influencing factors such as hydrate composition, residual water saturation (S_{rw}) and shut-in period during multistep depressurization were explored. Characteristics of CH_4 mole fraction in gas phase (XCH_4) were monitored, CH_4 recovery percent (RCH_4) and CO_2 storage ratio (SCO_2) during multistep depressurization were calculated in different operation conditions. Additionally, resistivity variation was studied to evaluate the effect of multistep depressurization on mixed hydrates saturation development.

2. Experimental methodology

2.1. Materials and apparatus

The mixed gas containing CH_4 (70 mol%) and CO_2 (30 mol%) and

Table 1
Information on injected mixed gas and prepared sandstone sample properties.

Exp no.	Gas used	Core no.	Sandstone properties					
			Dry weight/g	Diameter/cm	Length/cm	Density/g·cm^{-3}	Porosity/%	Initial water saturation/%
1	70%CH_4/CO_2	#4	71.74	2.55	7.20	2.60	24.96	81.9
2	30%CH_4/CO_2	#6	78.99	2.55	7.75	2.60	23.24	76.2
3	70%CH_4/CO_2	#5	79.31	2.55	7.75	2.60	22.93	82.2
4	70%CH_4/CO_2	#5	79.31	2.55	7.75	2.60	22.93	56.0
5	30%CH_4/CO_2	#7	81.93	2.55	7.75	2.60	20.38	88.6
6	30%CH_4/CO_2	#3	73.40	2.55	7.20	2.60	23.22	53.7
7	70%CH_4/CO_2	#3	73.40	2.55	7.20	2.60	23.22	54.2
8	70%CH_4/CO_2	#4	71.74	2.55	7.20	2.60	24.96	56.9

the other mixed gas of CH_4 (30 mol%) and CO_2 (70 mol%) were purchased from Air Liquide (Denmark). The deionized water was produced in the laboratory. A schematic of the experimental apparatus of mixed hydrate formation and exploitation is presented in Fig. 2. The significant parts of the apparatus were the core holder with a maximum working pressure of 200 bar. The prepared sandstone sample was wrapped by a rubber sleeve (Fig. 3) and placed at center of the core holder, sealed by an inlet and outlet cap, respectively. The core holder had a thermocouple at the outlet and two differential pressure indicators. Two alligator clips measuring the electrical resistance were placed at the inlet and outlet, respectively. Our previous work can refer to more information on electrical resistance measurement [45,55]. Gas cylinders injected different gases into sandstone samples through relief valves, control valves and supply lines. A high precision syringe pump (Teledyne ISCO) provided the sandstone sample with confining pressure by injecting deionized water to surround the rubber sleeve. A cooling bath controlled the system temperature by circulating antifreeze at the cooling jacket. Temperatures, pressures and electrical resistances were recorded by the data collector (Agilent 34972A, Agilent Tech.) at 10 s period. The gas samples were collected at the outlet of the core holder and analyzed by the in-line gas chromatograph (Micro-GC 490).

2.2. Core sample preparation

The preparation of the core sample included two parts: cleaning and saturating. The sandstone core was first washed with organic solvent (methanol and toluene) and then dried in an oven at 100 °C for 24 h. The dry weight of the sandstone core was subsequently recorded. For the core sample of low saturation, the dry sandstone core was immersed with ultrapure water in a beaker for 24 h. For the core sample of high saturation, the immersed sandstone core in a beaker was vacuumed simultaneously for 48 h, ensuring that the pores within the sandstone core were sufficiently degassed and thus saturated with water adequately. A prepared sandstone sample can be seen in Fig. 3. Core samples of different saturations using the preparation method above were obtained and summarized in Table 1.

2.3. Experimental procedure

2.3.1. Hydrate formation

The hydrate formation process in this study is consistent with our previous work [45]. The water-saturated core sample was wrapped tightly with a rubber sleeve and then packed into the core holder, with the inlet cap and the outlet cap pressing inwards. After connected the core holder with tubes and valves, the cooling bath was set to the desired temperature value. The core holder was flushed with target gas at 5 bar for 2 min to ensure the absence of air. Pressurization operation followed the following two steps: firstly, the desired confining pressure was achieved by water injection through ISCO pump; secondly, mixed gas was injected continually with the core pressure around 30 bar less than confining pressure. These two procedures were repeated for multiple injections until the confining pressure of 110 bar and core pressure of 70–90 bar were achieved. When the core pressure stabilized for 2 h at 22 °C, the temperature of the cooling bath was decreased to the experimental value. A noticeable pressure drop can be seen as the process of hydrate formation started. When the pressure of the core holder remained unchanged for 12 h, the hydrate formation process was determined to be completed. To improve water conversion into hydrate and hydrate distribution, a temperature ramping (multiple cooling and heating cycles within the temperature range of 1 °C and 22 °C) was employed [56,57]. Finally, if no pressure difference was seen between the inlet and outlet after temperature ramping operation, then the redistribution was regarded as completion totally inside the core sample due to adequate gas/liquid migration. Electrical resistance (R) between

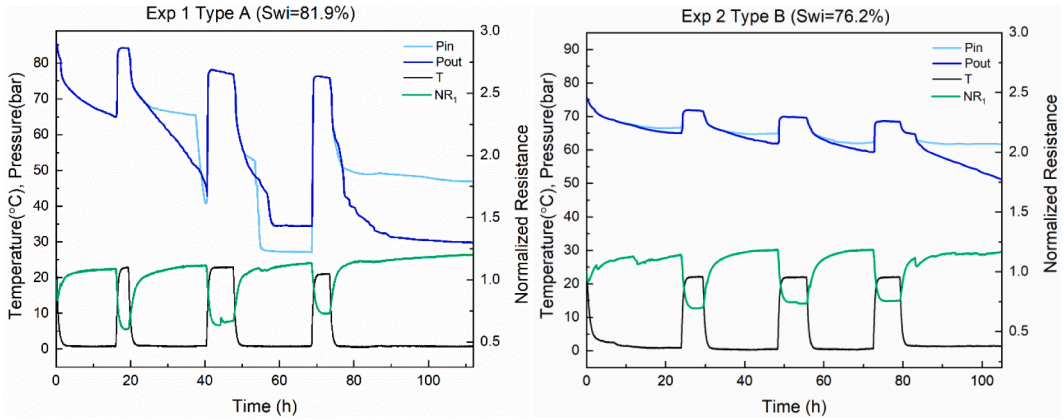

Fig. 4. Profiles of temperature (T), pressure (Pin & Pout) and NR1 during CH_4/CO_2 mixed hydrate formation in: (a) Exp1; and (b) Exp2.

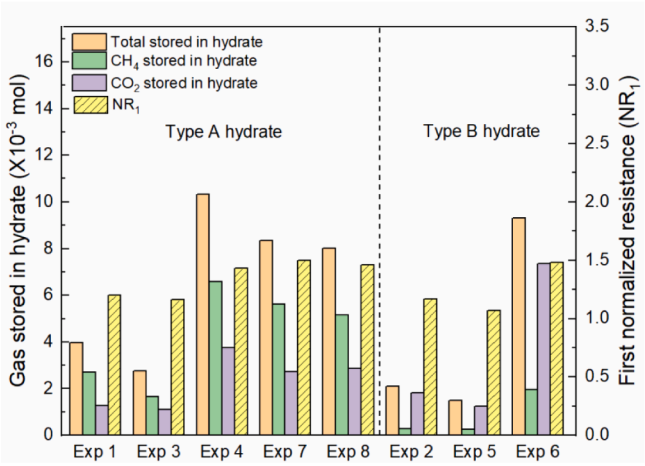

(a)

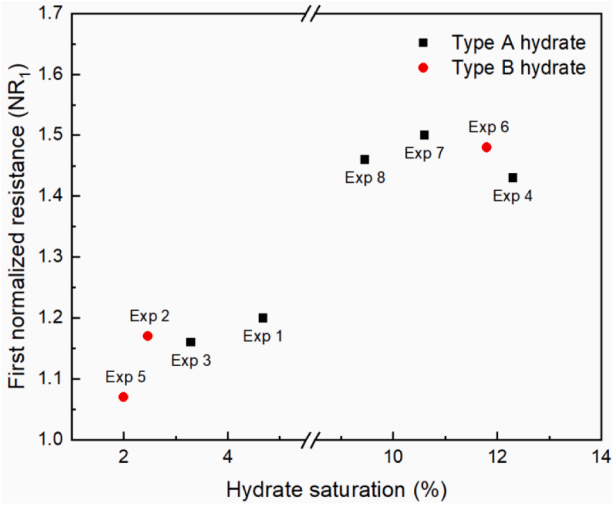

(b)

Fig. 5. A summary after mixed CH_4/CO_2 hydrate formation at different experiments: (a) total gas stored in hydrate, CH_4 in hydrate and CO_2 in hydrate, as well as NR_1; and (b) NR_1 to hydrate saturation.

the alligator clip 1 (inlet) and 2 (outlet), as well as pressure and temperature, were measured and recorded during the whole process. The R values were normalized during hydrate formation as the first normalization resistance (NR1); a detailed description can be found in the Ref. [45].

2.3.2. Multistep depressurization

After CH_4/CO_2 mixed hydrate formation, the following R values were normalized as second normalization resistance (NR_2). The position of the thermocouple was placed at the outlet, which can monitor the temperature change at the production site when employing multistep depressurization. Pressure drop at each depressurization stage was controlled by opening and closing the outlet value quickly, with the gas samples simultaneously collected and analyzed through the in-line micro gas chromatographer. Change of gas composition and resistivity were determined to investigate the dissociation characteristics of CH_4/CO_2 mixed hydrates, i.e. RCH_4, SCO_2, and percentage change of hydrate volume (Δ V) were calculated at the end of each depressurization according to mass balance. Percentage change of NR_2 before and after multistep depressurization (Δ NR_2) was calculated as well to analyze the variation of hydrate saturation during the multistep depressurization. The procedure of multistep depressurization proceeded with the pressure firstly decreased to CH_4 hydrate equilibrium pressure and then below it. This operation ceased until the value close to or under CO_2 hydrate equilibrium pressure. Noted that hydrate equilibrium was obtained from CSMGem for the bulk-only phase and it may differ in porous media. The hydrate equilibrium was assumed unchanged considering the reservoir temperature remained constant (small fluctuations in core temperature was ignored) during slow depressurization. Finally, the temperature was increased to 25 °C to dissociate all the hydrates.

3. Results and discussion

3.1. Profile of CH_4/CO_2 mixed hydrate formation

A detailed description of CH_4/CO_2 mixed hydrate formation can be referred to our previous publication [45]. In this work, similar strategies were used to generate mixed CH_4/CO_2 hydrates. The profiles of temperature, outlet pressure (P_{out}), inlet pressure (P_{in}), and first normalized resistance (NR_1) in different experiments have a similar trend. Fig. 4 shows the profiles of CH_4/CO_2 mixed hydrate formation in Exp1 and Exp2, respectively. It should be noted that the hydrate morphology is pore filling for water saturation higher than 35% [58]. A summary of moles stored in hydrate (total, CH_4 and CO_2), the value of NR_1, and the valve of NR_1 to hydrate saturation after mixed CH_4/CO_2 hydrate formation were showed in Fig. 5 (a) and Fig. 5 (b). More detailed information can be tracked in Table S1 of Appendix A.

In Fig. 4, sudden pressures were observed in the initial stage of hydrate formation for each cooling cycle. This was the sign of massive hydrate formation consuming CH_4/CO_2 mixed gas. Comparably, the following gentle pressure drops and final flat pressure lines were seen in the final stage of hydrate formation, which were caused by mass transfer barriers of hydrate films between water and gas molecules [33–35]. In Table S1 of Appendix A, the range of S_{wi} was 53.75–88.62% and it seemed that lower initial water saturation (S_{wi}) induced a more significant total amount of gas stored in hydrate, i.e. higher hydrate saturation (S_h). Noted that water diffusion plays a dominant role during hydrate formation and growth, in which hydrate films formed around water

Table 2
Information on multistep depressurization of mixed CH_4/CO_2 hydrates. S_{rw} and S_h are the residual water saturation and hydrate saturation before multistep depressurization. P_{CH4}, $P_{(CH4/CO2)}$ and P_{CO2} refer to the hydrate equilibrium pressures of CH_4, mixed CH_4/CO_2 right before multistep depressurization and CO_2, calculated from CSM [62].

Exp no.	Hydrate type	S_{rw}/%	S_h/%	Total steps of depressurization	Shut-in period/hour	Temperature/°C	P_{CH4}/bar	$P_{(CH4/CO2)}$/bar	P_{CO2}/bar
1	A	77.3	4.68	13	4	0.7	27.84	23.61	8.39
2	B	73.8	2.46	6	4	1.3	29.56	18.25	11.09
3	A	78.9	3.29	8	2	0.2	26.23	22.01	6.04
4	A	43.7	12.3	9	2	0.5	27.29	20.46	13.16
5	B	86.6	2.00	9	2	1.5	30.15	20.18	14.02
6	B	42.0	11.8	9	2	0.3	26.75	14.84	12.85
7	A	43.7	10.6	14	4	0.6	27.56	20.75	13.32
8	A	47.4	9.46	12	8	0.7	27.84	21.24	13.19

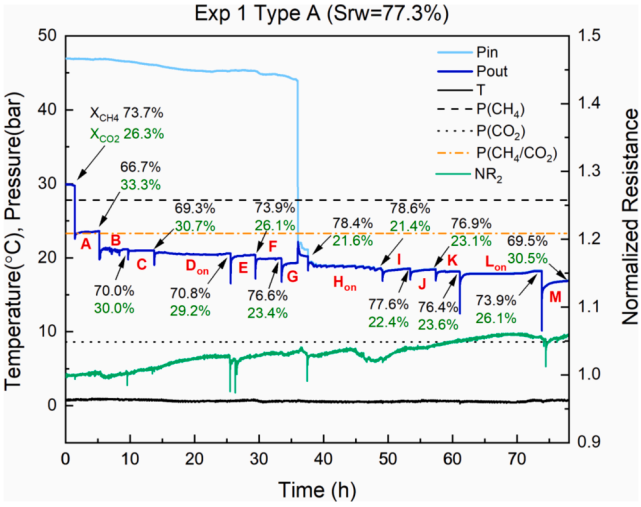

Fig. 6. Profiles of CH_4 and CO_2 mole fraction in collected gas samples (XCH_4 & XCO_2), pressure (P_{in} & P_{out}), temperature (T) and NR_2 during the multistep depressurization on Type A hydrate in Exp1. Shut-in period = 4 h, T = 0.7 °C, P_{CH4} = 27.84 bar, $P_{(CH4/CO2)}$ = 23.61 bar with 73.7 mol% CH_4/CO_2 gas right before the first depressurization, and P_{CO2} = 8.39 bar. D_{on} refers that Stage D proceeded overnight.

phase acting as diffusion barrier [34,59]. Comparably, CO_2 gas diffusion dominates the mass transfer during CH_4-CO_2 swapping on existing CH_4 hydrate [60,61]. Nevertheless, mixed hydrates of pure CH_4, pure CO_2 and CH_4/CO_2 coexisted in both cases in which hydrates formed from either mixed gases or CH_4-CO_2 swapping, although heterogeneity and micro properties differed.

It can be seen from Fig. 5 (a) that the mole of CH_4 in hydrate phase was higher than that of CO_2 in Exp1, Exp3-4 and Exp7-8, i.e., the mole ratio of CH_4 to CO_2 in the hydrate phase (RH) was greater than 1 shown in Table S1. This showed that mixed hydrates are rich in CH_4 and therefore classified as Type A. Comparably, the mole of CH_4 in hydrate phase was less than that of CO_2 in Exp2 and Exp5-6, which indicated that the CO_2-rich hydrates formed and thus were referred as Type B. Noted the values of RH for Type A hydrates (1.51–2.10) and Type B hydrates (0.15–0.27) were consistent with those calculated from CSMGem in Table S1. Additionally, a range of NR_1 (1.07 to 1.50) was observed, indicating an increase of hydrate saturation during CH_4/CO_2 mixed hydrate formation. Generally, it can be speculated from Fig. 5 (b) that higher hydrate saturation triggered higher NR_1 regardless of hydrate type. Nevertheless, the different amounts of CH_4 and CO_2 moles stored in mixed hydrates and heterogeneous hydrate distribution contributed to the difference of NR_1 within a range of similar hydrate saturation.

3.2. CH_4/CO_2 mixed hydrate dissociation

After synthesis of CH_4/CO_2 mixed hydrates of two types, different depressurization strategies were introduced. The detailed information on well-controlled manners is listed in Table 2. Next, different parameters including hydrate compositions, residual water saturation (S_{rw}), and shut-in period, were investigated for their correlations with CH_4 recovery and CO_2 storage. Specifically, Type A and Type B hydrates were synthesized in Exp1 and Exp2, respectively, to examine the effect of hydrate compositions on production and storage parameters during multistep depressurization. The effect of higher and lower S_{rw} was then studied in Exp3-6 to determine the value of S_{rw} that benefited CH_4 recovery and CO_2 storage for Type A and Type B hydrates. Finally, shut-in durations of 2 h (Exp4), 4 h (Exp7) and 8 h (Exp8) were employed to find a relatively beneficial selection for multistep depressurization on CH_4/CO_2 mixed hydrates.

3.2.1. Effect of hydrate composition

In realistic hydrate exploitation, CH_4/CO_2 mixed hydrates would exist at the CH_4 hydrate reservoir after CO_2 injection. In this case, kinetic inhibitors and anti-agglomerate chemicals are recommended to be added together with CO_2 injection to eliminate CO_2 plugging at the injection site. This could further improve CO_2 injectivity and allow a high CO_2 sweep range [37,63]. The following CO_2 migration from the injection site depends on permeability of hydrate-bearing sediment and relative permeability of CO_2, resulting in CO_2-water interface and CO_2-hydrate interface moving forward. This further induces formation and growth of both pure CO_2 hydrate and CH_4/CO_2 mixed hydrate. The CO_2 concertation decreases as the distance increases from injection site, causing CO_2-rich hydrates to enrich nearby the injection well and CH_4-rich hydrates to stay closer to the production well. As more CH_4 is produced from production well, CO_2 migration is driven from injection well to production well. This may alter the previous CH_4-rich hydrate zone into CO_2-rich one because of water and gas redistribution. Therefore, we investigated and compared the dissociation characteristics of CH_4-rich (Exp1) and CO_2-rich (Exp2) mixed hydrates, respectively. Additionally, the mole ratio of CH_4 to CO_2 in hydrate was 2.10 in Exp1 and 0.15 in Exp2, and the residual water saturation in Exp1 (77.3%) and Exp2 (73.8%) were similar. The shut-in period was controlled at 4 h between multistep depressurization. More information can be referred in Table 2 above and Table S1 of Appendix A.

Fig. 6 presents the profiles of CH_4 and CO_2 mole fraction in collected gas samples (XCH_4 & XCO_2), pressure (P_{in} & P_{out}), temperature (T) and second normalized resistance (NR_2) during the multistep depressurization on Type A hydrate in Exp1. It should be noted that P_{out} refers to depressurization pressure because pressure release was conducted in the outlet. Table S2 of Appendix A lists the values of those evaluation indicators at the end of different stages. The shut-in period was set to 4 h with a total of 13 pressure drops (Stage A to Stage M). It can be seen that the first drop was 6 bar, which brought the pressure to equilibrium pressure of mixed CH_4/CO_2 hydrate ($P_{CH4/CO2}$) at 0.7 °C. The following pressure drops were controlled at 3–4 bar (stage B to stage J) to explore the characteristics of multistep depressurization. The final pressure drops were made at 8 bar to approach the equilibrium pressure of CO_2 hydrate (P_{CO2}).

It was inspected that from Fig. 6 initial XCH_4 was 73.7 mol% before the multistep depressurization. This value decreased to 66.7 mol% at the end of Stage A without pressure rebound. Then XCH_4 increased as well as fluctuated around 70.0 mol% from Stage B and Stage D with pressure rebound. The increase of XCH_4 was attributed to the dissociation of CH_4-rich hydrate. It was noted that a pressure differential existed between outlet and inlet until stage G, in which a noticeable spike was detected on the outlet pressure curve. Pressure differential between outlet and inlet mainly redistributed gas and water in the pores. Subsequently, continuous pressure fluctuation was observed during Stage H and XCH_4 peaked at 78.6 mol% at the end of Stage H. This was caused by CH_4-rich hydrate dissociation and continuous fluid movement and gas-water mixing in the pore. It was noted water production occurred at the end of Stage L with obvious pressure rebound, which were produced by a large amount of CO_2-rich hydrates dissociation. This should be avoided because CO_2 release would reduce CO_2 storage efficiency and massive CO_2-rich hydrate loss may trigger instability of hydrate-bearing sediment. According to the Table S2 of Appendix A, a continuous increase of RCH_4 was observed at Exp1 from 72.0% at Stage A to 79.7% at Stage M. This was caused by gradual CH_4 hydrate dissociation when depressurization pressure was reduced gradually. However, actual CH_4 recovery efficiency would be decreased because of obvious XCH_4 decrease in the later steps of depressurization. The problematic issues of water production and dramatic XCH_4 decrease were therefore co-considered to cease multistep depressurization at selected stage.

In terms of enhanced CO_2 storage in Type A hydrates, SCO_2 experienced an increase before the end of Stage H with the highest value of 84.0% and then decreased slightly until the end of multistep

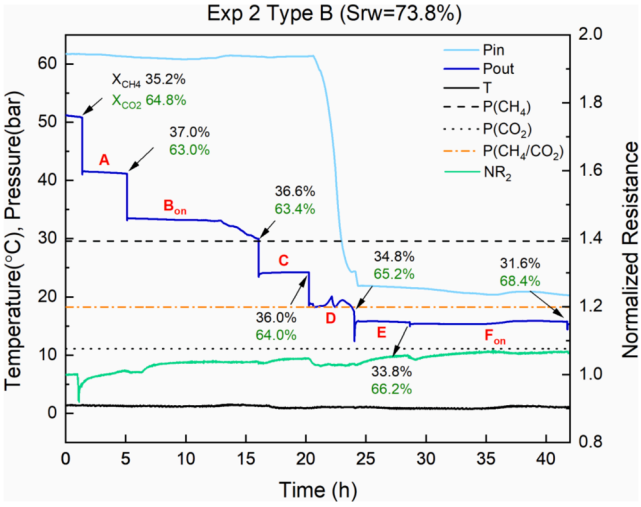

Fig. 7. Profiles of XCH_4 & XCO_2, P_{in} & P_{out}, T and NR_2 during the multistep depressurization on Type B hydrate in Exp2. Shut-in period = 4 h, T = 1.3 °C, P_{CH4} = 29.56 bar, $P_{(CH4/CO2)}$ = 18.25 bar with 35.2 mol% CH_4/CO_2 gas right before the first depressurization, P_{CO2} = 11.09 bar. B_{on} refers that Stage B proceeded overnight.

depressurization. This was because CO_2 initially formed hydrate with the depressurization pressure far beyond P_{CO2}. It was noted that SCO_2 started to drop since Stage I in Table S2. This was observed because those CO_2-rich hydrates started to dissociate even the depressurization pressure was 10 bar higher than P_{CO2}. Considering water production was observed during gas sample collected at the end of Stage L. Therefore, multistep depressurization was suggested to be terminated before this pressure release to avoid uncontrolled massive hydrate dissociation.

As can be seen in the Table S2 of Appendix A, negative value of ΔV in Exp1 hydrate meant a loss of hydrate mass volume during multistep depressurization. This was caused by the fact that the amount of CO_2 hydrate storage was fewer than that of CH_4 hydrate recovery. A relative minimal of ΔV (−56.28%) was realized at the end of Stage H, accompanied by the largest XCH_4 and SCO_2. This pressure point should be marked because enhancement of both CH_4 recovery and CO_2 storage was maximized. Nevertheless, it seems from Table S2 of appendix A that ΔNR_2 increased with more steps of depressurization. Although a decrease of hydrate saturation was observed according to the negative ΔV, the increased ΔNR_2 implied that multistep depressurization on CH_4/CO_2 mixed hydrates between P_{CH4} and P_{CO2} improved water-gas distribution along the core.

Fig. 7 shows the gas composition, pressure, temperature and NR_2 during the multistep depressurization on Type B hydrate in Exp2. Supplementary data can be referred to the Table S2 in Appendix A. It can be seen from Fig. 7 that the number of pressure drops was 6 in total (Step A to Step F). When the depressurization was performed from 50.8 bar to 41.2 bar, it can be seen that XCH_4 increased from 35.2 mol% at the beginning to 37.0 mol% at the end of Stage A. Since the pressure (41.2 bar) during Stage A was still higher than P_{CH4}, the slight increase of XCH_4 above was induced by CO_2-rich hydrate reformation, which was supported by a minimal pressure drop during Stage A. Noted that significant hydrate reformation was shown as sharp pressure drop just before the end of Stage B. The amount of CH_4 and CO_2 forming hydrate were equivalent, and therefore, the XCH_4 at the end of Stage B (36.6 mol %) was nearly equal to that at the end of Stage A (37.0 mol%).

It was noticed from Fig. 7 that the pressure differential between outlet and inlet occurred throughout the multistep depressurization. At the beginning of Stage D, a sudden pressure drop induced dissociation of CO_2-rich hydrates to release water and gas. On the one hand, this caused a 1.2 mol% increase of XCO_2. On the other hand, mass transfer was alleviated because of partial hydrate dissociation. Water and gas redistributed from outlet to inlet with time, causing hydrate dissociation and reformation along with the core, showed as pressure fluctuation during Stage D. The value of XCH_4 decreased from 34.8 mol% to 31.6 mol% from Stage D to Stage F. This was caused by the fact that the existing CO_2-rich hydrates tend to be unstable when depressurization pressure was close and below $P_{(CH4/CO2)}$. As a result, partial CO_2-rich hydrates dissociated and released more CO_2 than CH_4 and decreased XCH_4. Nevertheless, as seen in Table S2, RCH_4 increased from initial 30.4% as more CH_4 recovered with multistep depressurization. The highest RCH_4 was 81.2% acquired at the end of Stage F.

As for CO_2 storage for Type B hydrate in Exp2, an increasing trend of SCO_2 was observed with stages, and the highest SCO_2 was 82.8% nearly at the end of Stage E. Since the depressurization pressure was above PCO_2, CO_2-rich gas tended to form hydrate. The process of multistep depressurization was suggested terminated at the end of Stage E because massive water production occurred at the end of Stage F. The positive ΔV in Exp2 of Type B hydrate in Table S2 indicated a gain of hydrate mass volume during multistep depressurization on CO_2-rich hydrates, i.e. the amount of CO_2 reformation was larger than total loss of CH_4 hydrates. A maximal of ΔV (109.57%) was realized at the suggested ceasing point. Additionally, NR_2 increased with multistep depressurization indicating hydrate saturation in sediment increased.

According to the Table S2, the highest XCH_4 for Type A hydrate (78.6 mol% at 18.48 bar) was more than twice larger than those any value of XCH_4 for Type B hydrate, although RCH_4 at 18.48 bar for Type A hydrate (74.8%) was a lower than that for Type B hydrate (79.4%). This is important because CH_4-rich mixed gas can be applied after purification through an economical separation method, while CO_2-rich one was costly to be used [64,65]. In terms of CO_2 storage, the highest SCO_2 for Type A hydrate (84.0%) was slightly more than that for Type B hydrate (82.8%). It seemed that the Type A hydrate-bearing reservoir was dominated by CH_4 recovery while Type B by CO_2 storage through multistep depressurization according to the negative ΔV in Exp1 and positive ΔV in Exp2, respectively. However, ΔNR_2 values were both positive in Exp1 and Exp2, showing that sediment was stabilized with multistep depressurization operation. This can be understood that water gas transportation and distribution in the pore mainly affect the resistivity of hydrate-bearing sediment [51], although hydrate volume increased in Exp2 was mainly created by CO_2 hydrate reformation, whose resistivity is lower than CH_4 hydrate [52]. The results of negative ΔV in Exp1 and positive ΔV in Exp2 while both have increased NR_2 also indicated resistance was not directly correlated with mass volume but distribution that connected with fluid flow and water saturation. Therefore, the results above collectively indicated that it is better to perform multistep depressurization at the CH_4-rich hydrate zone to acquire and utilize CH_4 gas. This means the operation of multistep depressurization should cease before CH_4-rich hydrate changes into CO_2-rich one.

3.2.2. *Effect of residual water saturation*

Two types of hydrate deposits can be formed in porous media with different initial water saturation (S_{wi}), i.e. excess gas (S_{wi} < 50%) and excess water (S_{wi} > 50%). And excess water deposit may hinder gas production from depressurized hydrate reservoir [9]. It is noted that sandstones of high water saturation (>35%) generate hydrate morphology of pore-filling [58]. Therefore, Exp3-6 of excess water deposits (S_{wi} = 53.75–88.62%) were created with mass transfer barrier among pore water/gas and pore-filling hydrate affecting CH_4 recovery and CO_2 storage. During gas production from hydrate reservoir with higher water saturation, multiphase exits in the porous media and residual water saturation (S_{rw}) may be the dominant factor affecting heat transfer and mass transfer [66], and thus deciding CH_4 recovery and CO_2 storage by multistep depressurization. Therefore, the effect of different S_{rw} on multistep depressurization of CH_4/CO_2 mixed hydrate was investigated by performing experiments on Type A (Exp3 & Exp4) and Type B hydrate (Exp5 & Exp6), respectively. The mole ratio of CH_4 to

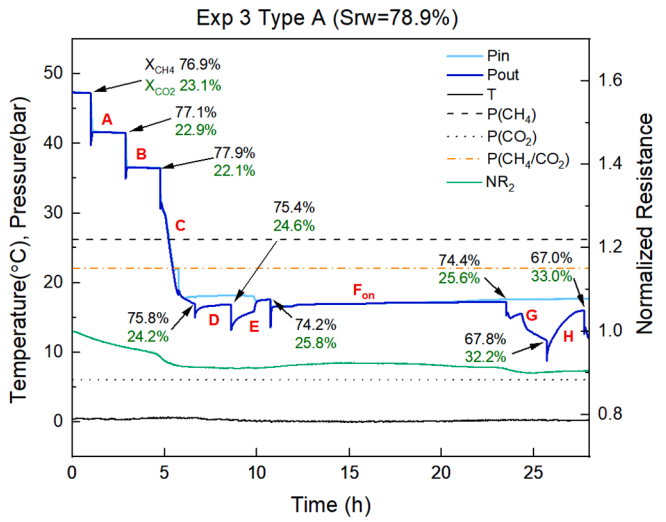

Fig. 8. Profiles of XCH_4 & XCO_2, P_{in} & P_{out}, T and NR_2 during the multistep depressurization on Type A hydrate with higher S_{rw} = 78.9% in Exp3. Shut-in period = 2 h, T = 0.2 °C, P_{CH4} = 26.23 bar, $P_{(CH4/CO2)}$ = 22.01 bar with 76.9 mol% CH_4/CO_2 gas right before the first depressurization, and P_{CO2} = 6.04 bar. F_{on} refers that Stage F proceeded overnight.

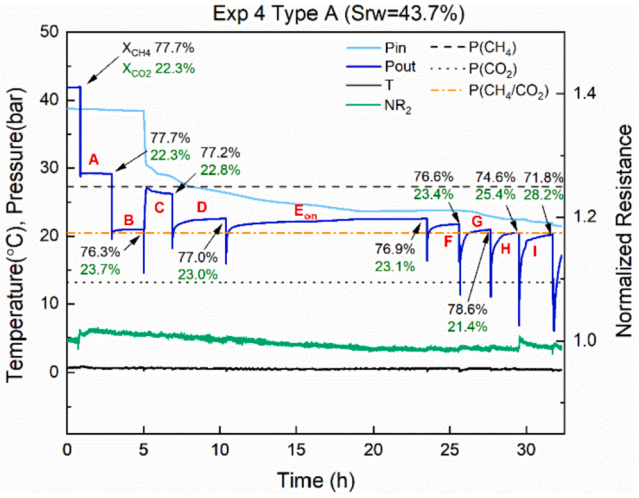

Fig. 9. Profiles of XCH_4 & XCO_2, P_{in} & P_{out}, T and NR_2 during the multistep depressurization on Type A hydrate with lower S_{rw} = 43.7% in Exp4. Shut-in period = 2 h, T = 0.5 °C, P_{CH4} = 27.29 bar, $P_{(CH4/CO2)}$ = 20.46 bar with 77.7 mol% CH_4/CO_2 gas before the first depressurization, P_{CO2} = 13.16 bar. E_{on} refers that Stage E proceeded overnight.

CO_2 in hydrate was 1.51 in Exp3 and 1.76 in Exp4, 0.21 in Exp5 and 0.27 in Exp6. The shut-in period was designed 2 h between multistep depressurization for Exp3-6, as described in Table 2 and Table S1 of Appendix A.

3.2.2.1. Type A mixed hydrate. In Exp3 of Type A hydrate sample, the higher S_{wi} of 82.2% triggered higher S_{rw} of 78.9% and lower S_h of 3.29% after hydrate formation. Fig. 8 shows the profiles of Type A mixed hydrate dissociation during multistep depressurization of 8 steps in Exp3. When performing multistep depressurization above P_{CH4} in Type A hydrate during Stage A and Stage B, no drastic change of XCH_4 was detected (only from 76.9 mol% to 77.9 mol%). This was caused by by slight CH_4-rich hydrate dissociation, as shown a pressure rebound appeared just after shut-in operation. A noticeable pressure drop occurred across the P_{CH4} line and the XCH_4 decreased from 77.9% to 75.8% during Stage C, indicating massive reformation of CH_4-rich hydrates. Subsequently, a pressure differential occurred between outlet and inlet, and XCH_4 was nearly unchanged during Stage D, showing nearly no gas composition change at the outlet. Water production was observed during gas collection at the end of Stage E, which can be predicted based on the pressure rise during Stage E as a result of massive hydrate dissociation. It was interesting to observe both dissociation and reformation of mixed hydrate with pressure increasing and decreasing during Stage G, while only hydrate dissociation dominated during Stage H with pressure rising.

When multistep depressurization was conducted between P_{CH4} and P_{CO2}, most CH_4-rich hydrates dissociated and contributed to RCH_4 recovery and CO_2-rich hydrate formed to enhance CO_2 storage. Practically, depressurization should controlled before Stage E in which water production started. To explore the highest values of RCH_4 and SCO_2 with the depressurization reduced close to P_{CO2}, further multistep depressurization was introduced after water production at the end of Stage E. It should be noted that pressure differences existed again during Stage G. This may be attributed to extreme inhomogeneity along the sandstone sample. Table S3 in the Appendix A illustrates the data of XCH_4, RCH_4, SCO_2, ΔV, and ΔNR_2 in Exp3. It can be seen that RCH_4 increased to peak values of 87.6% and SCO_2 increased to 86.2% at the end of Stage G. However, CO_2-rich hydrates occurred to dissociate significantly with depressurization pressure decreasing close to P_{CO2} at the end of Stage G, which was indicated as an obvious increase in pressure and a decrease in XCH_4 in Stage H, resulting in both decreases in RCH_4 and SCO_2. It was noted that water was continuously produced from Stage E to Stage H proving massive hydrates continuously dissociated, suggesting depressurization should be stopped before the end of Stage E. It can be seen from Table S3 that ΔV in Exp3 was negative, and its value decreased with time. This indicated that the amount of CH_4 recovered was greater than that of CO_2 stored over time. A negative range of ΔNR_2 (−2.6% to 9.9%) was also observed during multistep depressurization, confirming hydrate loss in hydrate-bearing sediment.

Comparatively, lower S_{rw}(43.7%) corresponded to higher S_h(12.32%) in the sandstone core was generated in Exp4 of Type A hydrate sample, the shut-in period was fixed at 2 h, same as in Exp3. A total of 9 steps of depressurizations was introduced, and each pressure drop was controlled with 8–12 bar. Fig. 9 describes the changes of hydrate dissociation characteristics for multistep depressurization in Exp4. More information can be tracked in Table S3 of the Appendix A. No change in XCH_4 was detected during Stage A because pressure was above $P_{CH4/CO2}$ and only free gas was removed. Noted that a pressure recovery was observed at the outlet in stage C due to the pressure difference existing between the outlet and the inlet. This pressure rebound allocated CH_4 and CO_2 between phases, causing noticeable declines in RCH_4 (from 77.2% to 67.6%) and SCO_2 (from 83.5% to 77.7%). Similar slight pressure increases were observed during Stage D-F, caused by continuous hydrate dissociation during shut-in period. The peak values of XCH_4 (78.6 mol%) and SCO_2 (85.1%) appeared at the end of Stage G, and then decreased gradually as a result of CO_2-rich hydrate dissociation caused by depressurization pressure performed below P_{CO2}. The phenomenon of water production appeared at the end of Stage G, which was the indicator of unwanted massive dissociation of hydrates and herby multistep depressurization needed to be terminated.

In Table S3 of Appendix A, the negative value of ΔV showed that the amount of CO_2 hydrate storage was less than that of the recovery of CH_4 hydrate during the whole depressurization. It was interesting ΔNR_2 that was initially positive at Stage A-D, indicating that multistep depressurization on lower S_{rw} hydrate sample improved gas water distribution at these stages. Subsequently, ΔNR_2 was negative since stage E, and the sediment became less stable with loss of hydrate saturation than before employing multistep depressurization. Nevertheless, the suggested ceasing point was selected at the end of Stage G with a relative lower ΔNR_2 of −1.2%.

It was inspected that Exp3 of higher S_{rw} was not suitable for

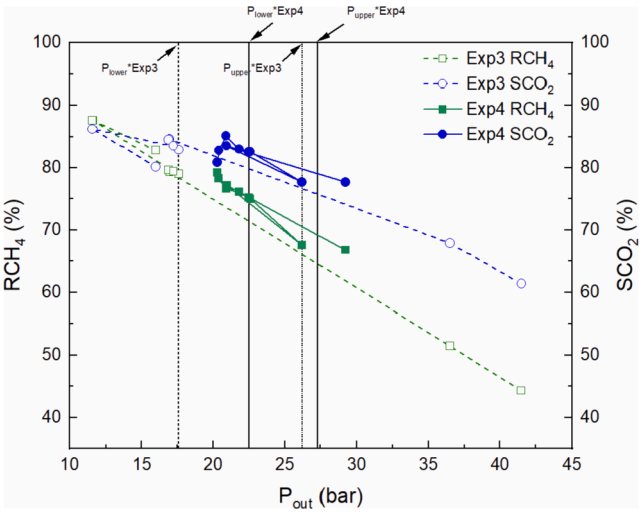

Fig. 10. Correlation between RCH_4 and SCO_2 with Pout in Exp3 of higher S_{rw} = 78.9% and Exp4 of lower S_{rw} = 43.7%. SCO_2 and RCH_4 were calculated using equations described in Appendix B.2.

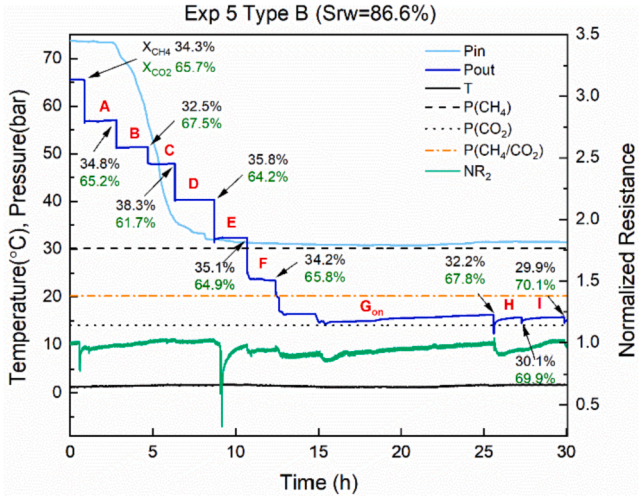

Fig. 11. Profiles of XCH_4 & XCO_2, P_{in} & P_{out}, T and NR_2 during the multistep depressurization on Type B hydrate with higher S_{rw} = 86.6% in Exp5. Shut-in period = 2 h, T = 1.5 °C, P_{CH4} = 30.15 bar, $P_{(CH4/CO2)}$ = 20.18 bar with 34.3 mol% CH_4/CO_2 gas right before the first depressurization, and P_{CO2} = 14.02 bar. G_{on} refers that Stage G proceeded overnight.

multistep depressurization because more hydrates dissociated and involved high risk of water production. Comparably, the drop in NR_2 was lower in Exp4 than Exp3, denoting that hydrate saturation was much more reserved and gas water distribution was improved in Exp4 of low S_{rw}. Fig. 10 presented the correlation between RCH_4 and SCO_2 with depressurization pressure (P_{out}) in Exp3 and Exp4. A depressurization pressure window was proposed for the controlled pressure release operation. Specifically, the upper pressure window (P_{upper}) was equal to PCH_4 and the lower pressure window (P_{lower}) was the ceasing pressure where water started to produce. When the depressurization pressure was reduced below P_{upper}, even though a higher RCH_4 of 79.0% was obtained in Exp3 at P_{lower} of 17.6 bar, much larger negative value of Δ NR_2 indicated huge loss of hydrate saturation in Exp3. This limited the application of multistep depressurization in such hydrate reservoir. Although lower RCH_4 of 75.2% was achieved in Exp4 at P_{lower} of 22.5 bar, less loss of hydrate mass and lower drop in Δ NR_2 allowed more effective depressurization than Exp3. The highest CO_2 storage ratio values were nearly the same in Exp3 (82.9%) and Exp4 (82.6%) at P_{lower},

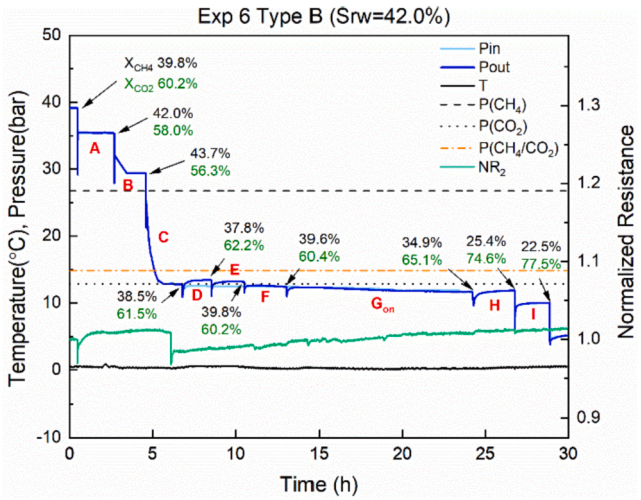

Fig. 12. Profiles of XCH_4 & XCO_2, P_{in} & P_{out}, T and NR_2 during the multistep depressurization on Type B hydrate with lower S_{rw} = 42.0% in Exp6. Shut-in period = 2 h, T = 0.3 °C, P_{CH4} = 26.75 bar, $P_{(CH4/CO2)}$ = 14.84 bar with 39.8 mol% CH_4/CO_2 gas just before the first depressurization, and PCO_2 = 12.85 bar. G_{on} refers that Stage G proceeded overnight.

indicating that both scenarios were potential selections for CO_2 storage. Collectively, multistep depressurization was highly proposed to improve CH_4 recovery from the CH_4-rich hydrate reservoir of lower S_{rw} and most of the CO_2 can be stored safely within the pressure window.

3.2.2.2. Type B mixed hydrate. The effect of different S_{rw} on dissociation manners of multistep depressurization was also investigated in Type B hydrates. Exp5 was conducted in Type B hydrate sample of higher S_{rw} = 86.6%. Fig. 11 presents the changes of CH_4/CO_2 in gas phase, pressure, temperature, and NR_2 in Exp5. A total of 9 depressurization steps was performed with each pressure drop of 6–10 bar, and the shut-in period was fixed at 2 h. More information can be found in the Table S4 in Appendix A.

Initially, the pressure was brought below P_{CH4} by performing 6 steps of depressurization at the outlet. It was observed that the inlet pressure was first above P_{out} and then plummeted below the corresponding P_{out}. This was caused by a slow water–gas distribution process along the length of sandstone. It was interesting that XCH_4 peaked at 38.3 mol% at stage C, where the P_{out} was equal to the P_{in}. It seemed that there was a blockage between the outlet and the inlet after stage E, since the pressure differential came and existed within the rest time. At the early stage of Stage G, two obvious pressure drops were inspected, indicating that CO_2-rich gas reformed hydrates as the pressure below $P_{(CH4/CO2)}$. This was supported by the indicators of SCO_2, which reached the highest values of 88.7% at the end of Stage G. The value of XCH_4 decreased significantly with more steps of depressurization at the pressure close to P_{CO2}. Nevertheless, it was observed that water production occurred at the end of Stage G and thus ceasing point was selected accordingly.

In Table S4 of Appendix A, the positive value of ΔV showed that Exp5 achieved more CO_2 hydrate storage than CH_4 hydrate recovery during the whole multistep depressurization. It was understood that CO_2-rich mixed gas tended to form CO_2-rich mixed hydrate with the pressure above P_{CO2}. ΔNR_2 was within the range of (−4.9% to 1.9%), except for a sharp decrease caused by short-term insulation failure in Stage E weakening the ΔNR_2 (−6.6% at the end of Stage F). The value of ΔNR_2 above illustrated that multistep depressurization of Type B hydrate of higher S_{rw} overall increased hydrate saturation and significantly improved gas water distribution along the core.

Exp.6 was the investigation of multistep depressurization characteristics in Type B hydrates of lower S_{rw} = 42.0%. A total of 9 stages of mixed hydrate dissociation were studied, with each pressure drop being

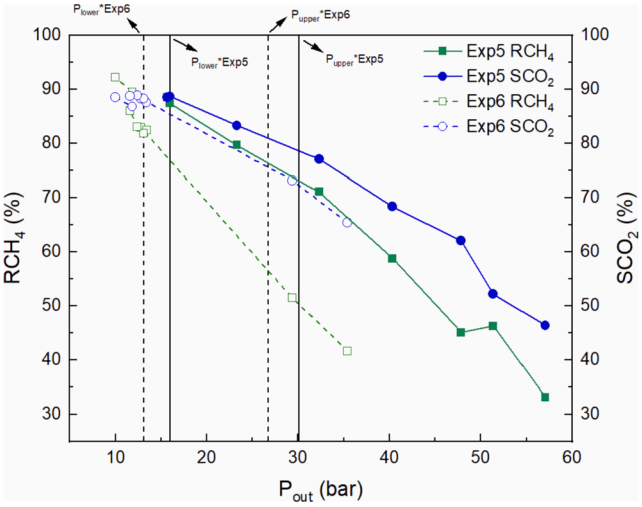

Fig. 13. The correlation between RCH_4 and SCO_2 with P_{out} in Exp5 of higher S_{rw} = 86.6% and Exp6 of lower S_{rw} = 42.0%. SCO_2 and RCH_4 were calculated using equations described in Appendix B.2.

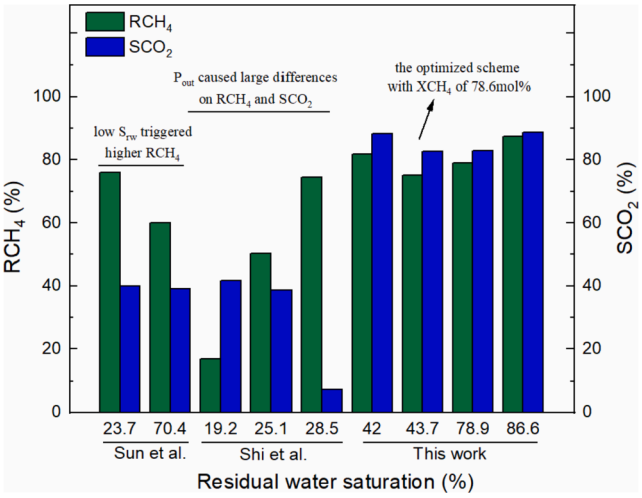

Fig. 14. Comparison of RCH_4 and SCO_2 in CO_2 swapping combined with depressurization from references and this work at different residual water saturation [53,67]. More details can be referred to Table S6 in Appendix A.

6–10 bar. The 2-hour shut-in period was used to perform the stepwise operations. Fig. 12 listed the detailed description of gas composition, pressure, temperature and NR_2 during multistep depressurization, and more data can be tracked in Table S4 of Appendix A.

In Fig. 12, the initial XCH_4 was 39.8 mol% before stage A. Subsequently, the depressurization pressures in Stage A and Stage B was decreased close to PCH_4, and thus the XCH_4 values were elevated to 42.0 mol% and 43.7 mol%. A significant pressure drop was observed during stage C, and XCH_4 was reduced to 38.5 mol%. This was caused by CH_4-rich hydrate reformation within stage C. The operating pressure fluctuated around P_{CO2} during Stage D and Stage E, having a marginal effect on the stability of CO_2-rich hydrates without obvious change of XCH_4. However, following depressurization was carried out during Stage F-I below P_{CO2}, causing CO_2-rich hydrates to dissociate and reduced XCH_4. It was noticed that water appeared at the end of Stage H and therefore depressurization should be closed before it. Exp6 also witnessed a positive ΔV during whole stages, indicating that more CO_2 was stored than CH_4 hydrate was recovered. ΔNR_2 was observed to be increasing with steps after Stage C, indicating an increase of hydrate saturation in terms of multistep depressurization on Type B hydrate of lower S_{rw}.

It was concluded from Table S4 that both ΔV were positive and ΔNR_2 increased with small fluctuations in Exp5 and Exp6, implying that Type B hydrate reservoirs of both higher S_{rw} and lower S_{rw} can be potential selection for multistep depressurization with slow manners. Fig. 13 showed the correlation between RCH_4 and SCO_2 with P_{out} in Exp5 of higher S_{rw} = 86.6% and Exp6 of lower S_{rw} = 42.0%. Regarding the depressurization pressure window of P_{upper} and P_{lower}, it can be seen that the highest SCO_2 was 88.7% for Exp5 of higher S_{rw} at P_{lower} of 15.97 bar, with a relative higher RCH_4 of 87.4%. The corresponding ΔV was 108.27% and ΔNR_2 was −1.9% at P_{lower}, which indicated hydrate saturation gain during multistep depressurization. Comparably, P_{lower} in Exp6 was 13.10 bar which was just above P_{CO2}, with the relative higher RCH_4 of 81.9% and SCO_2 of 88.3%. ΔNR_2 was only −0.8% and ΔV was 54.65% at this P_{lower} denoted increased hydrate saturation after multistep depressurization. As a reslut, Type B hydrate reservoirs of either higher S_{rw} or lower S_{rw} is able to achieve high efficiency of enhanced CH_4 recovery and CO_2 storage via multistep depressurization. According to the Table S4 in Appendix A, it may increase the economic competitiveness in Exp6 of low S_{rw} hydrate reservoir considering its higher XCH_4 of 39.8 mol% than 32.2 mol% in Exp5 of higher S_{rw}. Therefore, multistep depressurization was highly proposed for Type B hydrate of lower S_{rw}. And the multistep depressurization was suggested to be conducted within the pressure window to efficiently enhanced CH_4 recovery and CO_2 storage.

Fig. 14 summarizes the RCH_4 and SCO_2 in combination studies on CO_2 swapping with depressurization at different S_{rw} and compared the results with those in Section 3.2.2 in this work. It can be seen from Fig. 14 that the RCH_4 was 60% and 76% in Sun's work [67] conducting one-step depressurization and CO_2/H_2 injection. It was found that lower S_{rw} induced higher RCH_4 with the SCO_2 was nearly same at 40%. With a relatively lower S_{rw} of 19.2–28.5%, the range of RCH_4 was 17.1–74.4% and SCO_2 was 7.4–41.7% in Shi's [53] performing multistage depressurization after CO_2/N_2 swapping. The large differences between CH_4 recovery and CO_2 storage were caused by different multistage depressurization pressures. Overall, the RCH_4 and SCO_2 in Section 3.2.2 were was 75.2–87.4% and 82.6–88.7%, higher than those in the references. And no obvious trend was observed on CH_4 recovery and CO_2 storage as a function of S_{rw}. The optimized depressurization scheme was determined in Section 3.2.2 based on higher XCH_4 in produced gas without significant loss of hydrate volume, i.e. 78.6 mol% obtained at Type A hydrate of lower S_{rw} = 43.7%.

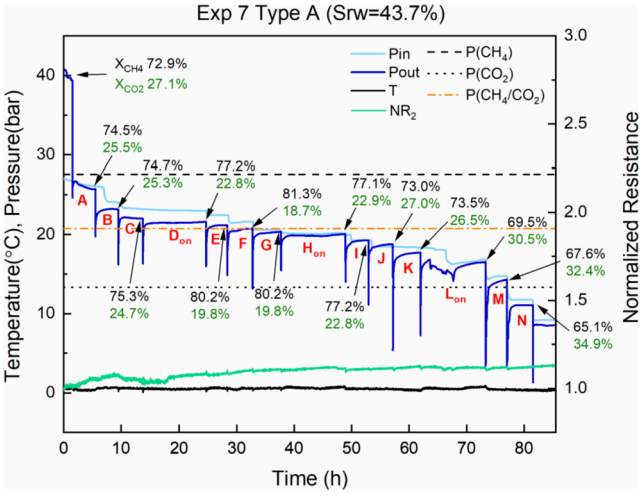

Fig. 15. Profiles of XCH_4 & XCO_2, P_{in} & P_{out}, T and NR_2 during the multistep depressurization on Type A hydrate in Exp7 of lower S_{rw} = 43.7%. Shut-in period = 4 h, T = 0.6 °C, P_{CH4} = 27.56 bar, $P_{(CH4/CO2)}$ = 20.75 bar with 72.9 mol% CH_4/CO_2 gas right before the first depressurization, and PCO_2 = 13.32 bar. D_{on} refers that Stage D proceeded overnight.

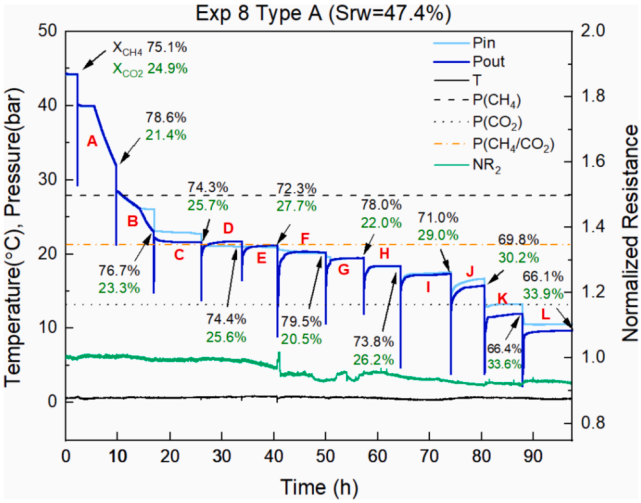

Fig. 16. Profiles of XCH_4 & XCO_2, P_{in} & P_{out}, T and NR_2 during the multistep depressurization on Type A hydrate in Exp8 of lower S_{rw} = 47.4%. Shut-in period = 8 h, T = 0.7 °C, P_{CH4} = 27.84 bar, $P_{(CH4/CO2)}$ = 21.24 bar with 75.1 mol% CH_4/CO_2 gas right before the first depressurization, and PCO_2 = 13.19 bar.

3.2.3. *Effect of shut-in period*

Extension of shut-in period can allow enough time for water and gas migration, which is dependent on capillary forces. This migration of water and gas helps to avoid the blockage of fluid flow channels and thus promoting hydrate dissociation and reformation. Meanwhile, multistep depressurization with sufficient shut-in period can allow sensible heat to transfer from reservoir to hydrate dissociation front and thus preventing unwanted ice formation. However, valuable production time can be wasted to pursue uneconomically enhanced CH_4 recovery and CO_2 storage using excessive shut-in period. The following work, therefore, extended the shut-in period to 4 h (Exp7) and 8 h (Exp8) in the CH_4-rich hydrate reservoir and compares the results with that of 2 h (Exp4). The aim was to find the highest XCH_4 and SCO_2, consider the total production time, and verify the resistance variation. It was known that S_{rw} was similar among experiments with 43.7% in Exp4 and Exp7, and 47.4% in Exp8. The mole ratio of CH_4 to CO_2 in hydrate was identical with 1.76 in Exp4, 2.06 in Exp7 and 1.80 in Exp8.

The shut-in period of 4 h was firstly selected, and a total of 14 steps were performed on Type A hydrate in Exp7. Profile of multistep depressurization on Type A hydrate in Exp7 can be analyzed in Fig. 15 and Table S5 of Appendix A. An increase in XCH_4 from 72.9 mol% to 74.5 mol% was inspected in Stage A with slight pressure decrease, induced by CO_2-rich hydrate reformation. Pressure rebounds were observed during Stage B-F with depressurization pressures just above $P_{(CH4\text{-}CO2)}$, indicating CH_4-rich hydrate dissociation. This brought the highest XCH_4 (81.3 mol%) at the end of Stage F. Afterwards, the depressurization pressure was below $P_{(CH4/CO2)}$ and approached P_{CO2}. This induced CO_2-rich hydrates unstable and started dissociating, causing XCH_4 to decline gradually until the final pressure below P_{CO2}. Water production was detected at the end of Stage J and ceasing point should be marked. It was noted that pressure fluctuation happened between outlet and inlet during Stage L. This implied that gas and water redistributed and transported as well as hydrate dissociation and reformation.

In terms of CO_2 storage evaluation, SCO_2 gradually increased from 74.6% at Stage A to the highest value of 85.3% at stage F because of CO_2-rich hydrate formation according to Table S5. After the depressurization pressure approached P_{CO2}, the existing CO_2-rich hydrates were more likely to dissociate, and therefore SCO_2 decreased since stage F. The exploitation time was considered 24 h for the highest XCH_4 and SCO_2 by counting 4-hour steps of 6 total. In Table S5 of Appendix A, the negative values of ΔV showed that the amount of CO_2 hydrate storage was fewer than that of CH_4 hydrate recovery. However, ΔNR_2 was positive throughout multistep depressurization, indicating that gas and water movement along the core significantly improved hydrate-containing sediment stability.

Fig. 16 shows the profiles of gas composition, pressure, temperature and NR_2 during the multistep depressurization in Exp8. The shut-in period was extended to 8 h with 12 steps of depressurization performed on Type A hydrate. Detailed information on XCH_4, RCH_4, SCO_2, ΔV, and ΔNR_2 can be found in Table S5 of Appendix A. The initial XCH_4 was 75.1 mol% at 44.2 bar before performing multistep depressurization. An immediate pressure rebounded and a slight pressure decrease were detected during stage A, with XCH_4 increasing to 78.6 mol%. This may be attributed to CO_2-rich hydrate forming initially. As the pressure reduced close to $P_{(CH4/CO2)}$, XCH_4 decreased to 76.7 mol% and 74.3 mol % at the end of stage B and stage C, respectively. This may be due to the fact that CH_4-rich hydrates were more likely to form than dissociation within a longer shut-in period. It was noted that a pressure differential existed during stage B and stage C, causing possible interactions of water and gas and heterogeneity of hydrate along with the sample.

When dissociation pressure was further decreased below $P_{(CH4/CO2)}$ and the pressure drop touched P_{CO2} since Stage F, a significant increase in XCH_4 was observed with a maximum value of 79.5 mol%, accompanied by the highest SCO_2 of 84.9% at the end of Stage F. Therefore, the operation time of 48 h was marked at the end of Stage F with the maximum XCH_4 and SCO_2. The explanation for the above phenomenon was that massive CH_4-rich hydrates dissociated CH_4 together with many CO_2-rich hydrates formed at the pressure below $P_{(CH4/CO2)}$. The following values of XCH_4 and SCO_2 declined with the next depressurization steps. RCH_4, however, still grew to the highest value of 90.3% throughout continuous hydrate exploitation until the end of multistep depressurization. It was noted that water production started coming at the end of Stage H and multistep production should be creased. The negative value of ΔV was the indicator of CH_4 hydrate recovery overnumbered CO_2 hydrate storage. Additionally, the negative value of ΔNR_2 showed that overall hydrate saturation was decreased correspondingly. This may be because too much CH_4 was recovered while CO_2 was not stored equivalently with a longer shut-in period of 8 h.

Table 3 summarizes the depressurization schemes and exploitation performances in Exp4, Exp7 and Exp8. It can be seen that different shut-in periods of 2 h-4 h-8 h affect the exploitation performance of CH_4/CO_2 mixed hydrates. At the suggested and optimized ceasing point, XCH_4 were the highest values of 78.6 mol%, 81.3 mol%, and 79.5 mol% for 2 h, 4 h, and 8 h, respectively, achieved at the depressurization pressures of 20.90 bar, 20.74 bar and 20.22 bar. The corresponding RCH_4 were

Table 3
Summary of depressurization schemes and exploitation performances in experiments with shut-in period of 2 h, 4 h and 8 h at the targeted ceasing point, P_{out} is the depressurization pressure, XCH_4 is the mole fraction of CH_4 in gas phase, RCH_4 is the CH_4 recovery percent, and SCO_2 is the CO_2 storage ratio. ΔV is the percentage change of hydrate volume and ΔNR_2 is the percentage change of normalized resistance.

Exp	Shut-in period (h)	P_{out} (bar)	Total production time (h)	XCH_4 (mol%)	RCH_4 (%)	SCO_2 (%)	ΔV (%)	ΔNR_2 (%)
4	2	20.90	14	78.6	76.6	85.1	−65.71	−1.2
7	4	20.74	24	81.3	72.6	85.3	−63.86	10.2
8	8	20.22	48	79.5	75.0	84.9	−73.91	−6.7

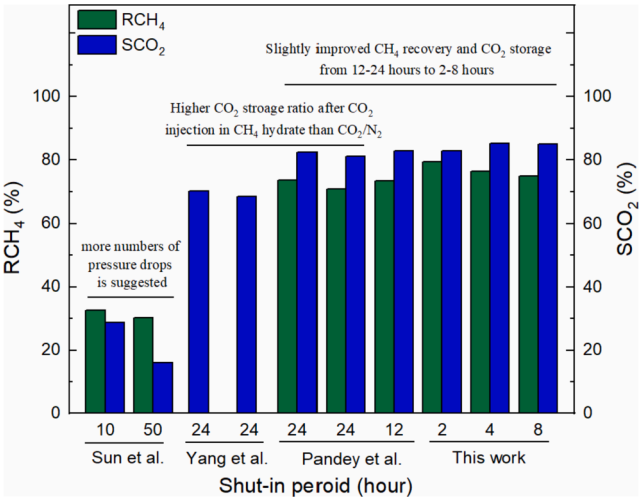

Fig. 17. Comparison of RCH_4 and SCO_2 in CO_2 swapping combined with depressurization from references and this work at different shut-in period [31,41,45]. More details can be referred to Table S6 in Appendix A.

76.6%, 72.6%, and 75.0%. It is expected to see that the highest XCH_4 came with the highest SCO_2 (85.1%, 85.3% and 84.9 % for 2 h, 4 h and 8 h), which were nearly same and indicated that most CO_2 could form hydrates and remained stable during multistep depressurization at the pressure close to $P_{(CH4/CO2)}$. This meant that the most suitable depressurization schemes achieved simultaneous the highest efficiency of CH_4 recovery and CO_2 storage at the targeted ceasing pressure, with the total production time were 10 h, 24 h and 48 h for Exp4, Exp7 and Exp8, respectively. The ΔV values for these three were almost same (−65.71%, −63.86% and −73.91% for 2 h, 4 h and 8 h), indicating a total loss of hydrate volume. However, the value of ΔNR_2 was 10.2% for 4 h, which was higher than the negative values for 2 h (−1.2%) and 8 h (−6.7%). This means that hydrate-bearing sediment was improved through efficient gas water movement and distribution within core samples after multistep depressurization with 4-hour shut-in period.

Fig. 17 compares the RCH_4 and SCO_2 in combination studies of CO_2 swapping with depressurization from references and Section 3.2.3 in this work. It can be inspected from Sun's work [31] that higher numbers of pressure drops with shorter shut-in period was more beneficial to CH_4 production and CO_2 retention. The SCO_2 in Yang's [41] was lower than those in Pandey's [45], which was resulted from $CH_4/CO_2/N_2$ mixed hydrate in Yang's and CH_4/CO_2 mixed hydrates in Pandey's. This indicated that multistep depressurization was suggested to be performed after CO_2 injection in CH_4 hydrates for higher efficiency of CO_2 storage. It seemed that reducing shut-in period can improve CH_4 recovery and CO_2 storage slightly in terms of 24-hour and 12-hour cases in Pandey's. Nevertheless, the RCH_4 can be further enhanced from 71.0% to 73.8% to 75.0–79.4%, and SCO_2 from 81.0% to 82.9% to 82.8–85.1%, respectively through reducing shut-in period from 12 h to 24 h to 2–8 h. This indicated that sufficient water and gas migration can be completed within a much shorter shut-in period (2–8 h) for efficient CH_4 recovery and CO_2 storage. But too long shut-in period (12–24 h) without depressurization may cause less efficiency on CH_4-rich hydrate decomposition and CO_2-rich hydrate reformation than those with shorter ones (2-8 h).

3.3. Comparison of efficiency and practical implication

Fig. 18 summarizes the changes of XCH_4, SCO_2, and RCH_4 with P_{out} during multistep depressurization at Exp1-8. The assumptions and equations used to calculate SCO_2 and RCH_4 were described in the Appendix B. Noted that the lowest P_{out} was the point at which the multistep depressurization should be ceased as discussed above. As seen in Fig. 18 (a–c), the maximum values of XCH_4 for Type A hydrate were 74–82 mol %, while those for Type B hydrate were 37–44 mol%. The maximum value of XCH_4 (81.3 mol%) was observed in Exp7, accompanied by the peak SCO_2 at the end P_{out} of 20.74 bar. No obvious differences in peaked SCO_2 values were observed between Type A hydrate (84–87%) and Type B hydrate (83–89%) in Fig. 18(d–f), indicating that majority of CO_2 in all scenarios can be stored as hydrate in sediment by multistep depressurization. And SCO_2 can be enhanced generally with the reduced depressurization pressure at the conditions that CO_2-rich hydrates can form thermodynamically. According to Fig. 18(g–i), the maximum value of RCH_4 seemed to depend mainly on P_{out}. When P_{out} was decreased close to 10 bar, the maximum value of RCH_4 can be greater than 80% in Exp2, 3, 5–6. Compared to Exp1, 4, 7–8, when P_{out} was reduced to about 20 bar, the maximum value of RCH_4 was less than 80%. This was following the fact that more CH_4 can be recovered with the increase of depressurization step and the decrease of depressurization pressure.

When hydrates dissociate by depressurization in a porous medium, continuous mixing occurs between the liquid and gaseous phases due to capillary forces, differences in relative permeability, and mobilization of pore water. In a mixed hydrate system with two different hydrates (CH_4 and CO_2 hydrate of different composition), the CH_4 hydrate can remain stable outside its stability zone because it is surrounded by a more stable CO_2 hydrate layer. Therefore, the pressure response and production behaviors are influenced by the mass transfer barrier of the CO_2 hydrate as well as the presence of two stability zones, resulting in the likelihood of hydrate reformation. This gives the mixed hydrate system additional stability compared to a pure CH_4 hydrate system [46].

Generally, four types of dissociation and reformation characteristics during multistep depressurization mainly affecting CH_4 recovery and CO_2 storage can be recognized in this work, as summarized in Fig. 19. When the depressurization pressures were reduced below $P_{(CH4/CO2)}$ and above $P_{(CO2)}$, obvious wanted CH_4-rich hydrate dissociation and CO_2-rich hydrate reformation can be observed according to the profiles of pressure rebound and sharp decrease. Gas concentration changes regarding XCH_4 and XCO_2 also supported the explanation above. A similar phenomenon of pressure rebound was reported in the schemes of slow stepwise depressurization [30] and intermittent depressurization [68], which significantly contributed to the CH_4 production. In addition, the pressure rebounded to just above $P_{(CH4/CO2)}$ at CH_4-rich hydrate dissociation, indicating that further depressurization may improve CH_4 recovery continuously. Noted that the gas compositions were collected and acquired at the end of each multistep depressurization while this dynamic hydrate dissociation-reformation, as well as water-gas distribution, may occur at any time during the shut-in period. In contrast, when the depressurization pressures were operated below $P_{(CO2)}$ or above $P_{(CH4/CO2)}$, unwanted CO_2-rich hydrate dissociation or CH_4-rich hydrate reformation were detected based on variations of pressure and CH_4/CO_2 fraction. The reforming CH_4-rich hydrates were not problematic because they can be recovered with the depressurization pressure reduced below $P_{(CH4/CO2)}$. However, the dissociating CO_2-rich hydrates should be avoided to decrease the efficiency of CH_4 recovery and CO_2 storage. These four types of pressure and gas composition characteristics can be employed to verify the occurrence of hydrate reformation and dissociation, thus enhancing CH_4 production and CO_2 retention via depressurizing stepdown pressure between $P_{(CH4/CO2)}$ and $P_{(CO2)}$.

In a more realistic production field, CH_4 recovery and CO_2 storage should be considered comprehensively because the former is related to the direct profit of CH_4 product, and the latter can save undirected costs by CO_2 sequestration. These two indicators, therefore, are being maximized. Additionally, the production time for the multistep depressurization is critical concerning the costly operation cost on the platform. Meanwhile, the stability of hydrate-bearing sediment needs to be maintained through increased hydrate saturation or improved gas water distribution. Fig. 20 is the combined analysis of SCO_2 to increase of CH_4 concentration (ΔXCH_4), P_{out} to $P_{(CH4/CO2)}$, and production time to ΔNR_2 at the optimized conditions in this work. From the perspective of higher

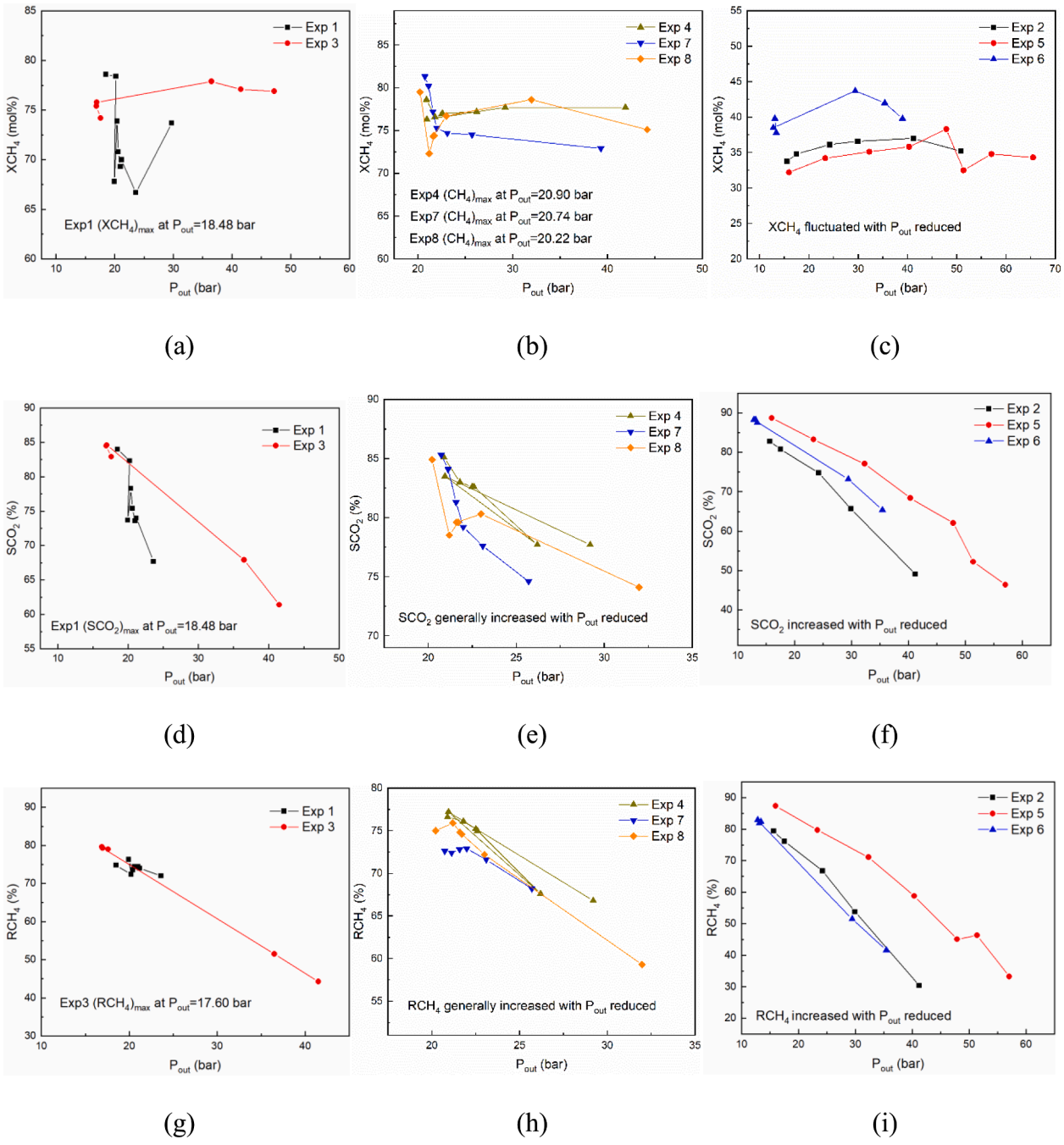

Fig. 18. Summary of dissociation characteristics during multistep depressurization at Type A hydrate (Exp1, 3, 4, 7–8) and Type B hydrate (Exp2, 5–6) with the lowest P_{out} as the ceasing point: (a–c) XCH_4 with P_{out}; (d–f) SCO_2 with P_{out} and, (g–i) RCH_4 with P_{out}. SCO_2 and RCH_4 were calculated using equations described in Appendix B.2.

enhancement of CH_4 recovery and CO_2 storage, it can be speculated that Exp1, Exp4, Exp7, and Exp8 should be highlighted with the positive values of ΔXCH_4 (>0 mol%) and SCO_2 (> 84.0%) simultaneously shown in Fig. 20(a). These positive ΔXCH_4 and higher SCO_2 values were obtained by performing multistep depressurization until P_{out} was close to or just below the equilibrium pressure of mixed CH_4/CO_2 hydrates, shown in Fig. 20(b). Among these best four experiments, Exp7 emerged as the highest value ΔNR_2(10.2%) with a shorter production time (24 h: 4-h shut-in × 6 stages) in total, as indicated in Fig. 20(c). It should be noted that Exp1 was also marked as its ΔNR_2 was of positive value (2.3%), however, the production time (32 h: 4-h shut-in × 8 stages) was relatively longer. Therefore, the 4-hour shut-in period may be the best option to enhance CH_4 recovery and CO_2 storage simultaneously during multistep depressurization in the CH_4-rich hydrate reservoir.

The scheme of an injection well and a production well to explore NGHs by swapping CH_4-CO_2 in the reservoir is highly recommended in the realistic production trial. Specifically, CO_2 is delivered to the reservoir from the injection well, while CH_4-rich gas is collected from the production well by depressurization. Herein, CH_4-rich hydrates around the production well tend to become CO_2-rich by dissociating and reformation hydrates with the risk of water production. Furthermore, further depressurization in the production well may yield lean CH_4 gas effluent, which needs to be costly to acquire a CH_4 gas product. Our work is concerned with the above issues and determines the patterns of different multistep depressurization. A suitable operation strategy of a 4-hour shut-in period with a production pressure close to $P_{(CH4/CO2)}$ is

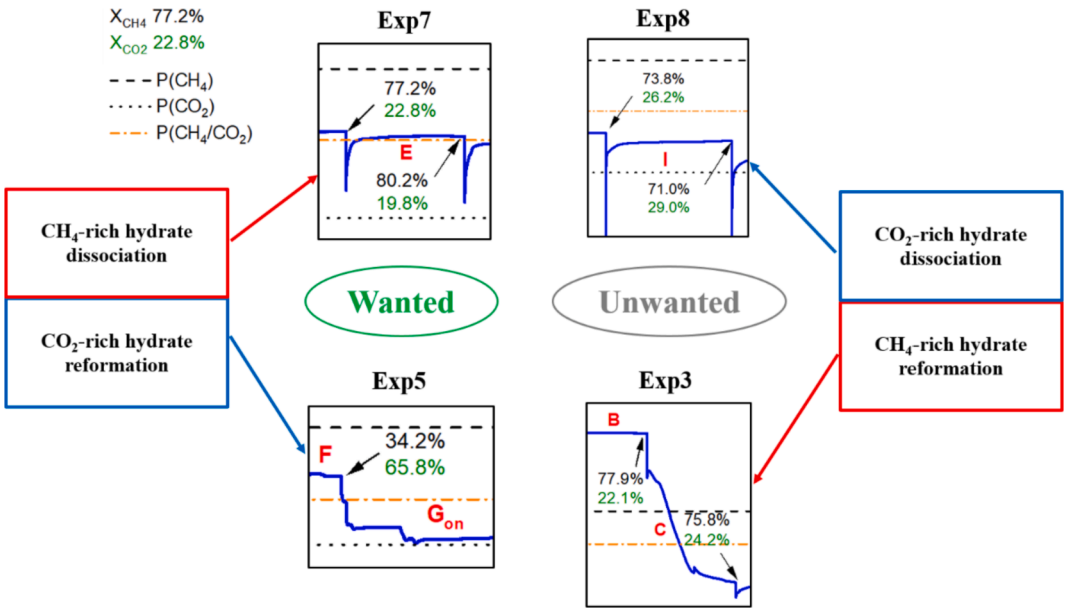

Fig. 19. Four types of dissociation and reformation characteristics during multistep depressurization.

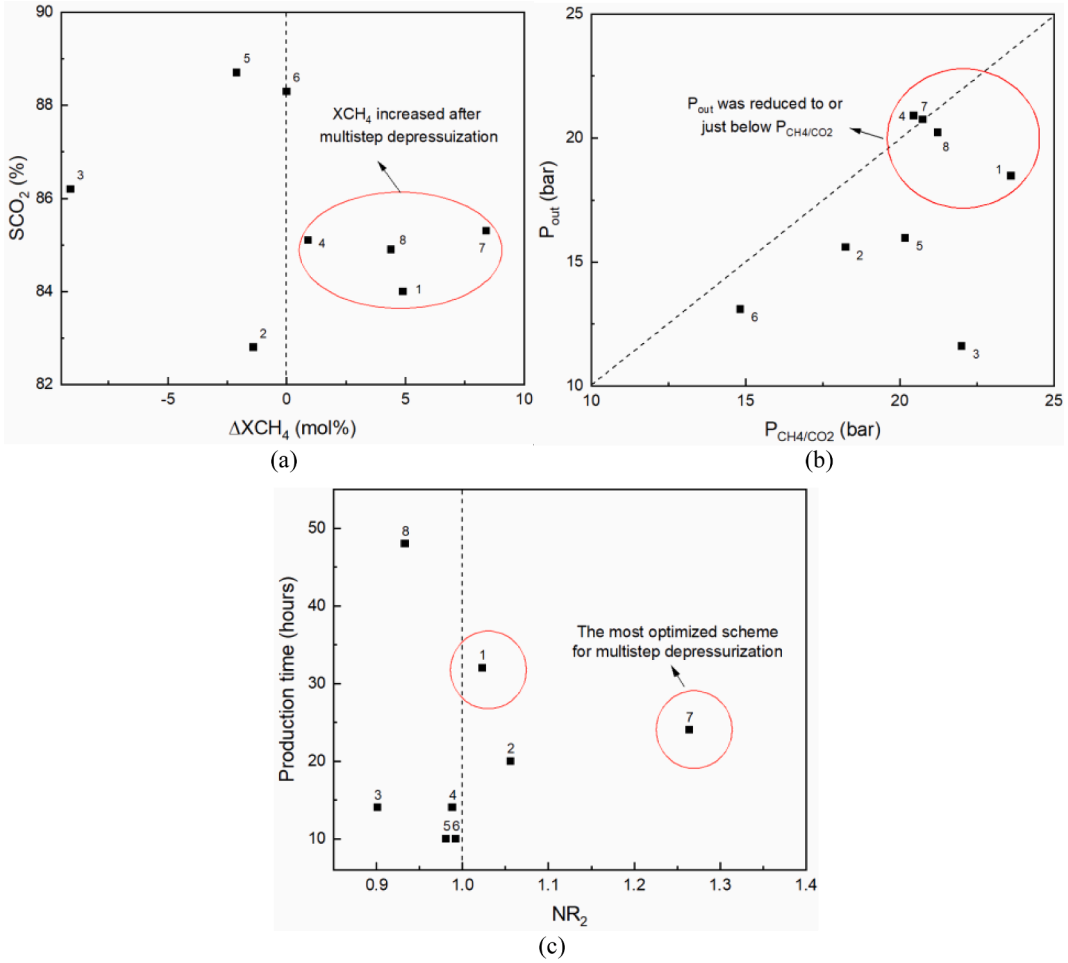

Fig. 20. Comprehensive comparisons at the optimized conditions of: (a) SCO_2 to ΔXCH_4, (b) P_{out} to $P_{(CH4/CO2)}$ and, (c) production time to ΔNR_2. ΔXCH_4 and ΔNR_2 were calculated using equations described in Appendix B.2.

Table S1
Formation data at different experiments. P_i and T_i are initial pressure and temperature before hydrate formation. S_{wi} is initial water saturation. P_f and T_f are final pressure and temperature after hydrate formation. ΔP is the pressure drop during hydrate formation. S_{rw} and S_h refer to residual water saturation and hydrate saturation after hydrate formation. V_h is hydrate volume after hydrate formation. $nCH_4(H)$, $nCO_2(H)$, $nCH_4(G)$ and $nCO_2(G)$ are the mole of CH_4 and CO_2 in hydrate phase and gas phase, respectively. $RH(CH_4/CO_2)$ refers to the mole ratio of CH_4 to CO_2 in hydrate phase. $RH(CH_4/CO_2)_{CSM}$ refers to the $RH(CH_4/CO_2)$ calculated from CSMGem software [62]. NR_1 is the first normalized resistance after mixed hydrate formation. Type A hydrate is CH_4-rich and Type B hydrate is CO_2-rich.

	Exp1	Exp2	Exp3	Exp4	Exp5	Exp6	Exp7	Exp8
P_i/bar	75.90	68.45	82.10	89.90	89.34	73.30	80.80	83.40
T_i/℃	21.06	22.10	24.00	21.88	21.90	23.00	22.00	21.81
S_{wi}/%	81.93	76.20	82.20	55.97	88.62	53.75	54.22	56.87
P_f/bar	29.70	50.83	47.20	41.90	65.50	39.00	39.30	44.20
T_f/℃	0.85	1.40	0.40	0.80	1.26	0.47	0.47	0.80
ΔP/bar	46.20	17.62	34.90	48.00	23.84	34.30	41.50	39.20
S_{rw}/%	77.3	73.8	78.9	43.7	86.6	42.0	43.7	47.4
S_h/%	4.68	2.46	3.29	12.3	2.00	11.8	10.6	9.46
V_h/cm^3	0.43	0.23	0.30	1.12	0.16	1.01	0.90	0.87
$nCH_4(H)/\times10^{-3}$mol	2.69	0.27	1.66	6.58	0.26	1.96	5.61	5.16
$nCO_2(H)/\times10^{-3}$mol	1.28	1.82	1.10	3.75	1.24	7.34	2.72	2.86
$nCH_4(G)/\times10^{-3}$mol	4.45	2.67	4.67	13.12	1.79	5.32	11.24	11.85
$nCO_2(G)/\times10^{-3}$mol	1.28	1.82	1.10	3.75	1.24	7.34	2.72	2.86
$RH(CH_4/CO_2)$	2.10	0.15	1.51	1.76	0.21	0.27	2.06	1.80
$RH(CH_4/CO_2)_{CSM}$	2.96	0.52	2.78	1.40	0.75	0.28	1.41	1.44
NR_1	1.20	1.17	1.16	1.43	1.07	1.48	1.50	1.46
Hydrate type	A	B	A	A	B	B	A	A

Table S2
Pressure, XCH_4, RCH_4, SCO_2, ΔV and ΔNR_2 at different stages of multistep depressurization in Exp1-2. XCH_4 is the mole fraction of CH_4 in gas phase. RCH_4 is the CH_4 recovery percent. SCO_2 is the CO_2 storage ratio. ΔV is the percentage change of hydrate volume and ΔNR_2 is the percentage change of normalized resistance. The suggested ceasing stage was marked with bold.

Exp 1 Type A (Srw=77.3%)							Exp 2 Type B (Srw=73.8%)						
Stage	Pout	XCH_4	RCH_4	SCO_2	ΔV	ΔNR_2	Stage	Pout	XCH_4	RCH_4	SCO_2	ΔV	ΔNR_2
	bar	mol%	%	%	%	%		bar	mol%	%	%	%	%
	29.70	73.7						50.83	35.2				
A	23.60	66.7	72.0	67.7	−59.77	0.1	A	41.20	37.0	30.4	49.1	88.26	1.1
B	21.16	70.0	74.0	74.0	−59.53	0.1	B	29.90	36.6	53.8	65.7	99.57	3.4
C	20.98	69.3	74.4	73.6	−60.23	0.8	C	24.20	36.1	66.8	74.8	105.65	4.7
D	20.59	70.8	74.4	75.4	−59.53	1.6	D	17.50	34.8	76.1	80.8	108.70	3.1
E	20.39	73.9	73.6	78.3	−57.21	2.8	**E**	**15.60**	**33.8**	**79.4**	**82.8**	**109.57**	**5.6**
F	19.92	67.8	76.3	73.7	−62.56	3.2	F	15.70	31.6	81.2	82.5	106.52	6.8
G	20.20	78.4	72.4	82.3	−53.95	2.5							
H	**18.48**	**78.6**	**74.8**	**84.0**	**−56.28**	**2.3**							
I	18.54	77.6	75.1	83.2	−56.98	4.0							
J	18.43	76.9	75.5	82.8	−57.67	4.4							
K	18.16	76.4	75.6	82.4	−57.91	5.1							
L	18.20	73.9	76.6	80.8	−60.00	5.6							
M	16.88	69.5	79.7	79.2	−64.42	5.5							

proposed for the original CH_4 hydrate reservoir. After the CH_4-rich hydrate reservoir is transformed into CO_2-rich by depressurization exploitation, multistep depressurization on CO_2-rich hydrates should be avoided from the economic point of view due to the lean effluent of CH_4. Related to the initial water saturation, hydrate saturation appears to be less critical than operation modes and hydrate compositions, depending on the production performance. Furthermore, water production can signify massive dissociation of CO_2 hydrates, and therefore, multistep depressurization must cease before the pressure decreases close to P_{CO2}.

As shown in the ΔNR_2 results, either hydrate saturation or water gas distribution was improved overall after multistep depressurization. However, the distribution of water, gas and mixed hydrates needs to be further investigated to know their effects on sediment stability. A further investigation employing magnetic resonance imaging (MRI) or x-ray microcomputed tomography (CT) to characterize fluid distribution in the core needs to be combined to better understand multistep depressurization on mixed hydrates.

4. Conclusion

The multistep depressurization on CH_4/CO_2 hydrates was intensively investigated to enhance CH_4 recovery and CO_2 storage. The effects of three critical parameters: hydrate compositions (Type A and Type B hydrate), residual water saturation (S_{rw}), and shut-in period (2 h, 4 h and 8 h) were studied to evaluate the gas compositions, CH_4 recovery and CO_2 storage efficiency, water gas distribution in hydrate-bearing sediment during multistep depressurization. The conclusions are summarized below.

- To maximize CH_4 recovery and CO_2 storage with higher CH_4 molar fraction in the gas phase (XCH_4) and CO_2 storage ratio (SCO_2), it was highly recommended to perform multistep depressurization on Type A hydrates (CH_4/CO_2 ratio of 1.76–2.06) of low S_{rw} (43.7–47.4%).
- Depressurization was suggested reduced in steps and controlled at a certain pressure window to achieve wanted CH_4-rich hydrate dissociation and CO_2-rich hydrate reformation without water production. The final ceasing pressure was found close to the equilibrium pressure of CH_4/CO_2 mixed hydrates concerning the initial gaseous CH_4/CO_2 composition.
- With combined consideration of efficiency and production time, the highest XCH_4 reached 81.3 mol% and the corresponding SCO_2 was 85.3% through 6-step depressurization with 4-hour shut-in period,

Table S3
Pressure, XCH_4, RCH_4, SCO_2, ΔV and ΔNR_2 at different stages of multistep depressurization in Exp3-4. XCH_4 is the mole fraction of CH_4 in gas phase. RCH_4 is the CH_4 recovery percent. SCO_2 is the CO_2 storage ratio. ΔV is the percentage change of hydrate volume and ΔNR_2 is the percentage change of normalized resistance. The suggested ceasing stage was marked with bold.

Exp 3 Type A (Srw=78.9%)							Exp 4 Type A (Srw=43.7%)						
Stage	Pout	XCH_4	RCH_4	SCO_2	ΔV	ΔNR_2	Stage	Pout	XCH_4	RCH_4	SCO_2	ΔV	ΔNR_2
	bar	mol			%	%		bar	mol			%	%
Before	47.20	76.9	–	–	–	–	Before	41.90	77.7	–	–	–	–
A	41.50	77.1	44.3	61.4	−30.26	−2.6	A	29.20	77.7	66.8	77.7	−55.54	1.5
B	36.50	77.9	51.5	67.9	−37.70	−4.4	B	20.95	76.3	77.2	83.5	−67.32	1.0
C	16.95	75.8	79.3	84.6	−72.38	−7.9	C	26.20	77.2	67.6	77.7	−56.70	0.7
D	16.89	75.4	79.6	84.5	−72.98	−8.7	D	22.60	77.0	75.0	82.6	−64.73	0.0
E	**17.60**	**74.2**	**79.0**	**82.9**	**−73.06**	**−8.6**	E	22.50	76.9	75.2	82.6	−64.91	−1.4
F	17.22	74.4	79.4	83.5	−73.42	−8.6	F	21.80	76.6	76.1	83.0	−66.07	−1.3
G	11.61	67.8	87.6	86.2	−85.13	−9.9	**G**	**20.90**	**78.6**	**76.6**	**85.1**	**−65.71**	**−1.2**
H	15.99	67.0	82.8	80.2	−81.42	−9.7	H	20.40	74.7	78.3	82.8	−69.20	−1.5
							I	20.30	71.8	79.2	80.9	−71.43	−1.9

Table S4
Pressure, XCH_4, RCH_4, SCO_2, ΔV and ΔNR_2 at different stages of multistep depressurization in Exp5-6. XCH_4 is the mole fraction of CH_4 in gas phase. RCH_4 is the CH_4 recovery percent. SCO_2 is the CO_2 storage ratio. ΔV is the percentage change of hydrate volume and ΔNR_2 is the percentage change of normalized resistance. The suggested ceasing stage was marked with bold.

Exp 5 Type B (Srw=86.6%)							Exp 6 Type B (Srw=42.0%)						
Stage	Pout	XCH_4	RCH_4	SCO_2	ΔV	ΔNR_2	Stage	Pout	XCH_4	RCH_4	SCO_2	ΔV	ΔNR_2
	bar	mol%	%	%	%	%		bar	mol%	%	%	%	%
Before	65.50	34.3	–	–	–	–	Before	39.00	39.8	–	–	–	–
A	57.00	34.8	33.2	46.4	73.14	−3.1	A	35.40	42.0	41.6	65.4	52.57	0.8
B	51.39	32.5	46.3	52.2	70.57	−0.8	B	29.40	43.7	51.5	73.2	55.74	1.2
C	47.87	38.3	45.1	62.1	97.17	1.7	C	12.80	38.5	82.9	88.3	54.06	−1.6
D	40.34	35.8	58.8	68.4	94.83	1.9	D	13.40	37.8	82.4	87.6	53.56	−1.2
E	32.28	35.1	71.1	77.1	100.65	−2.5	**E**	**13.10**	**39.8**	**81.9**	**88.3**	**54.65**	**−0.8**
F	23.32	34.2	79.7	83.3	104.85	−6.6	F	12.40	39.6	83.0	88.9	54.75	−0.7
G	**15.97**	**32.2**	**87.4**	**88.7**	**108.27**	**−1.9**	G	11.60	34.9	86.0	88.8	52.77	0.8
H	15.67	30.1	88.5	88.5	106.56	−4.9	H	11.85	25.4	89.5	86.8	48.12	1.2
I	15.70	29.9	88.5	88.5	106.34	0.4	I	9.99	22.6	92.2	88.5	48.51	1.2

Table S5
Pressure, XCH_4, RCH_4, SCO_2, ΔV and ΔNR_2 at different stages of multistep depressurization in Exp7-8. XCH_4 is the mole fraction of CH_4 in gas phase. RCH_4 is the CH_4 recovery percent. SCO_2 is the CO_2 storage ratio. ΔV is the percentage change of hydrate volume and ΔNR_2 is the percentage change of normalized resistance. The suggested ceasing stage was marked with bold.

Exp 7 Type A (Srw=43.7%)							Exp 8 Type A (Srw=47.4%)						
Stage	Pout	XCH_4	RCH_4	SCO_2	ΔV	ΔNR_2	Stage	Pout	XCH_4	RCH_4	SCO_2	ΔV	ΔNR_2
	bar	mol%	%	%	%	%		bar	mol%	%	%	%	%
Before	39.30	72.9	–	–	–	–	Before	44.20	75.1	–	–	–	–
A	25.70	74.5	68.2	74.6	−62.86	5.2	A	31.98	78.6	59.3	74.1	−54.37	0.2
B	23.10	74.7	71.6	77.6	−66.41	6.5	B	23.00	76.7	72.2	80.3	−72.07	−0.4
C	21.99	75.3	72.9	79.2	−67.52	3.8	C	21.60	74.3	74.8	79.6	−76.67	−0.7
D	21.58	77.2	72.8	81.3	−66.19	7.9	D	21.70	74.4	74.6	79.6	−76.32	−0.8
E	21.13	80.2	72.4	84.1	−64.19	8.6	E	21.20	72.3	75.9	78.5	−79.08	−3.0
F	**20.74**	**81.3**	**72.6**	**85.3**	**−63.86**	**10.2**	**F**	**20.22**	**79.5**	**75.0**	**84.9**	**−73.91**	**−6.7**
G	20.32	80.2	73.5	84.8	−65.52	10.7	G	19.50	78.0	76.3	84.4	−76.44	−4.7
H	20.22	77.1	74.7	82.4	−68.51	11.4	H	18.37	73.8	78.9	82.5	−81.72	−5.3
I	19.22	77.2	75.9	83.5	−69.84	11.0	I	17.34	71.0	80.9	81.8	−85.29	−7.2
J	18.75	73.0	77.8	80.8	−73.95	11.4	J	15.75	69.8	83.0	82.8	−88.16	−8.5
K	17.70	73.5	78.9	82.3	−74.94	12.5	K	11.97	66.4	87.8	85.7	−94.48	−8.1
L	16.49	69.5	81.5	81.1	−79.38	11.5	L	9.70	66.1	90.3	88.4	−96.90	−7.6
M	14.27	67.6	84.5	82.7	−83.04	11.8							
N	11.03	65.1	88.7	85.8	−87.58	12.1							

and the depressurization pressure was reduced to 20.74 bar on Type A hydrates of 43.7% S_{rw}.

- The positive values of normalized resistance percent change (ΔNR_2) after multistep depressurization was correlated with S_{rw} and shut-in period. A suitable shut-in period of 4 h was most beneficial to both enhanced production performances and improved gas water distribution.

CRediT authorship contribution statement

Qian Ouyang: Writing – original draft, Investigation, Formal analysis, Validation, Visualization, Data curation. **Jyoti Shanker Pandey:** Conceptualization, Methodology, Supervision, Writing – review & editing. **Nicolas von Solms:** Supervision, Project administration, Funding acquisition.

Table S6
Summary of depressurization schemes in the literatures for comparison in this work. RCH_4 is the CH_4 recovery percent. SCO_2 is the CO_2 storage ratio. XCH_4 is the mole fraction of CH_4 in gas phase.

Reference	Water saturation (%)	Pressure drop (bar)	Shut-in period (hours)	Production performances
Sun et al. [67]	23.7	37-20	none	$RCH_4 = 76\%$, $SCO_2 = 40\%$
	70.4	37-20	none	$RCH_4 = 60\%$, $SCO_2 = 39\%$
Shi et al. [53]	19.2	145-102-64	~100	$RCH_4 = 17.1\%$, $SCO_2 = 41.7\%$
	25.1	106-81-67	~100	$RCH_4 = 50.3\%$, $SCO_2 = 38.6\%$
	28.5	85-53-33	~100	$RCH_4 = 74.4\%$, $SCO_2 = 7.4\%$
Sun et al. [31]	38.8	29.2-17.4-29.2-17.4-29.2-17.4	50	$RCH_4 = 30.3\%$, $SCO_2 = 16.0\%$
	38.8	29.2-17.4	10	$RCH_4 = 32.7\%$, $SCO_2 = 28.8\%$
Yang et al. [41]	11.5	42-39-35-31-28-25	24	$XCH_4 = 85\text{mol}\%$, $SCO_2 = 70.4\%$
	19.6	71-57-49-41	24	$XCH_4 = 91\text{mol}\%$, $SCO_2 = 68.5\%$
Pandey et al. [45]	44.7	37.3-24.3-24.1-24.0	24	$RCH_4 = 73.8\%$, $SCO_2 = 82.4\%$
	34.4	52.5-41.4-26.2	24	$RCH_4 = 71.0\%$, $SCO_2 = 81.0\%$
	53.2	41.1-32.8-21.0-20.6-20.3	10	$RCH_4 = 73.6\%$, $SCO_2 = 82.9\%$

Declaration of Competing Interest

The authors declare that they have no known competing financial interests or personal relationships that could have appeared to influence the work reported in this paper.

Acknowledgement

This work is supported by the Department of Chemical and Biochemical Engineering, Technical University of Denmark, and the Scholarship of Guangzhou Elite Plan. The authors appreciate Tran Thuong Dang for his technician assistance and Xu Li for figure improvement in this work.

Appendix A

See Tables S1–S6.

Appendix B. Calculation of experimental data

B.1. Hydrate formation

The moles of mixed hydrates ($n_{CH_4,H}, n_{CO_2,H}$) formed at core holder can be given using Eqs. (1) and (2):

$$n_{CH_4,H} = n_{CH_4,i} - n_{CH_4,f} \tag{1}$$

$$n_{CO_2,H} = n_{CO_2,i} - n_{CO_2,f} \tag{2}$$

where ($n_{CH_4,i}$, $n_{CO_2,i}$) and ($n_{CH_4,f}$, $n_{CO_2,f}$) are the moles of CH_4 and CO_2 in the gas phase at the starting point before and ending point after hydrate formation; they can be determined using the following Eqs. (3)–(8):

$$n_{CH_4,i} = n_{mix,i} \times \chi_{CH_4,i} \tag{3}$$

$$n_{CO_2,i} = n_{mix,i} \times \chi_{CO_2,i} \tag{4}$$

where $\chi_{CH_4,i}$ and $\chi_{CO_2,i}$ are the gas mole fraction of CH_4 and CO_2 initially. $n_{mix,i}$ is the mole amount of mixed gas in the sandstone, which can be calculated:

$$n_{mix,i} = \frac{P_i V_i}{Z_i R T_i} \tag{5}$$

where P_i is the initial pressure at core after mixed gas injection and V_i is the gas volume inside the core. Z_i is the compressibility factor of mixed gas at a given temperature and pressure, calculated from Benedict–Webb–Rubin–Starling equation of state. R is the universal gas constant and T_i is the initial temperature at the outlet of the core holder.

Considering CH_4/CO_2 mixed hydrates occurs inside the core with a constant gas volume, moles of CH_4 ($n_{CH_4,f}$) and CO_2 ($n_{CO_2,f}$) in the gas phase after hydrate formation are calculated:

$$n_{CH_4,f} = n_{mix,f} \times \chi_{CH_4,f} \tag{6}$$

$$n_{CO_2,f} = n_{mix,f} \times \chi_{CO_2,f} \tag{7}$$

$$n_{mix,f} = \frac{P_f V_i}{Z_f R T_f} \tag{8}$$

where $\chi_{CH_4,f}$ and $\chi_{CO_2,f}$ are the mole fraction of CH_4 and CO_2 gas components after hydrate formation. $n_{mix,f}$ Refers to the mole amount of residual mixed gas within the core, calculated from the same gas equation of state using Eq. (8).

In terms of the hydrate composition at the end of hydrate formation, the mole amount of CH_4 in the hydrate phase ($\Delta n_{CH_4,H}$) and that of CO_2 ($\Delta n_{CO_2,H}$) is given by Eqs. (9) and (10):

$$\Delta n_{CH_4,H} = n_{CH_4,i} - n_{CH_4,f} \tag{9}$$

$$\Delta n_{CO_2,H} = n_{CO_2,i} - n_{CO_2,f} \tag{10}$$

B.2. Hydrate dissociation

Three indicators are employed to evaluate the performance of mixed hydrate dissociation, i.e. CH_4 recovery percentage R_{CH_4}(%), CO_2 storage ratio S_{CO_2}(%), hydrate volume percent change ΔV (%), and normalized resistance percent change ΔNR_2 (%). The total CH_4 recovery percentage is calculated using the flowing equations based on different stages of mixed hydrate stability:

$$R_{CH_4} = \frac{n_{CH_4,Re}}{n_{CH_4,H} + n_{CH_4,f}} \times 100\% \tag{11}$$

$n_{CH_4,Re}$ is the total CH_4 mole released during multistep depressurization, which can be obtained based on the mass balance and assumption calculation below:

$$n_{CH_4,Re} = \left(\Delta n_{CH_4,H} + n_{CH_4,f}\right) - \left(\Delta n_{CH_4,step} + n_{CH_4,v1}\right) \tag{12}$$

where $\left(\Delta n_{CH_4,H} + n_{CH_4,f}\right)$ is the total mole of CH_4 at the beginning of multistep depressurization. $\Delta n_{CH_4,step}$ and $n_{CH_4,v1}$ are the mole amount of CH_4 remaining in the hydrate and gas phases at the end of multistep depressurization, respectively. When the dissociation pressure is below the CH_4 hydrate equilibrium pressure, it can be assumed that all CH_4 are recovered, and no CH_4 are left in the hydrate phase ($\Delta n_{CH_4,step} = 0$) in terms of the CH_4 released during multistep depressurization. And $n_{CH_4,v1}$ can be obtained by:

$$n_{CH_4,v1} = y_{CH_4,v1} \frac{P_{v1} V_i}{Z_{v1} R T_{v1}} \tag{13}$$

where $y_{CH_4,v1}$ is the mole fraction of CH_4 in the gas phase after the multistep depressurization.

The corresponding total CO_2 storage ratio S_{CO_2}(%) can be given:

$$S_{CO_2} = \frac{n_{CO_2,St}}{n_{CO_2,H} + n_{CO_2,f}} \times 100\% \tag{14}$$

$n_{CO_2,St}$ is the total CO_2 mole stored in hydrate during cyclic depressurization, which can also be obtained based on the mass balance calculation:

$$n_{CO_2,St} = \left(\Delta n_{CO_2,H} + n_{CO_2,f}\right) - \left(\Delta n_{CO_2,re} + n_{CO_2,v1}\right) \tag{15}$$

where $\left(\Delta n_{CO_2,H} + n_{CO_2,f}\right)$ is the total mole of CO_2 at the beginning of multistep depressurization.$\Delta n_{CO_2,re}$ is the mole amount of CO_2 recovered together with CH_4-rich gas. When the dissociation pressure is above the CO_2 hydrate equilibrium pressure, CO_2 gas is enriched in the hydrate phase as CO_2 hydrate reformation. It can be assumed that the recovered amount of CO_2, together with CH_4-rich gas released from CH_4 hydrate dissociation, can be ignorable $\Delta n_{CO_2,re} = 0$. $n_{CO_2,v1}$ is the mole amount of CO_2 in gas phase at the end of multistep depressurization given by:

$$n_{CO_2,v1} = y_{CO_2,v1} \frac{P_{v1} V_i}{Z_{v1} R T_{v1}} \tag{16}$$

where $y_{CO_2,v1}$ is the mole fraction of CO_2 in the gas phase after the multistep depressurization.

The hydrate volume percent change ΔV is introduced to investigate the percentage change of mixed hydrate mass, with a positive value of ΔV indicating hydrate mass increase and negative one means hydrate mass decrease.

$$\Delta V = \frac{\left(\Delta V_{CO_2(St)} - \Delta V_{CH_4(Re)}\right)}{V_H} \times 100\% \tag{17}$$

where V_H is the hydrate volume before multistep depressurization, $\Delta V_{CO_2(St)}$ and $\Delta V_{CH_4(Re)}$ refer to the volumes of CO_2 stored, and CH_4 released,

respectively and given by Equation (18-20):

$$V_H = \frac{\Delta n_{CO_2,H} M_w N}{\rho_{CO_2,H}} + \frac{\Delta n_{CH_4,H} M_w N}{\rho_{CH_4,H}} \quad (18)$$

$$\Delta V_{CO_2(St)} = \frac{n_{CO_2,St} M_w N}{\rho_{CO_2,H}} \quad (19)$$

$$\Delta V_{CH_4(Re)} = \frac{n_{CH_4,Re} M_w N}{\rho_{CH_4,H}} \quad (20)$$

where M_w is the mole mass of water (18 g/mol), and N is the hydrate number (6.00). And $\rho_{CO_2,H}$ (0.9 g/cm^3) and $\rho_{CH_4,H}$ (1.1 g/cm^3) are the density of CO_2 hydrate and CH_4 hydrate [1].

The increase of CH_4 concentration (Δ XCH_4) is calculated as followed:

$$\Delta\chi_{CH_4} = \chi_{CH_4,lower} - \chi_{CH_4,f} \quad (21)$$

where $\chi_{CH_4,lower}$ is the mole fraction of CH_4 in the gas phase at the suggested ceasing point, $\chi_{CH_4,f}$ is the mole fraction of CH_4 in the gas phase before multistep depressurization.

The normalized resistance percent change ΔNR_2 is defined as followed:

$$\Delta NR_2 = \frac{NR_{2,f} - NR_{2,i}}{NR_{2,i}} \times 100\% \quad (22)$$

where $NR_{2,f}$ is the value of normalized resistance at the end of each stage and $NR_{2,i}$ is the corresponding value before multistep depressurization.

References

[1] Sloan ED, Koh CA. Clathrate Hydrates of Natural Gases. CRC Press 2007.
[2] Vedachalam N, Ramesh S, Jyothi VBN, Thulasi Prasad N, Ramesh R, Sathianarayanan D, et al. Evaluation of the depressurization based technique for methane hydrates reservoir dissociation in a marine setting, in the Krishna Godavari Basin, east coast of India. J Nat Gas Sci Eng 2015;25:226–35.
[3] Sun Y, Li B, Guo W, Lü X, Zhang Y, Li K, et al. Comparative analysis of the production trial and numerical simulations of gas production from multilayer hydrate deposits in the Qilian Mountain permafrost. J Nat Gas Sci Eng 2014;21:456–66.
[4] Boswell R, Collett TS. Current perspectives on gas hydrate resources. Energy Environ Sci 2011;4:1206–15. https://doi.org/10.1039/c0ee00203h.
[5] Piñero E, Marquardt M, Hensen C, Haeckel M, Wallmann K. Estimation of the global inventory of methane hydrates in marine sediments using transfer functions. Biogeosciences 2013;10:959–75. https://doi.org/10.5194/bg-10-959-2013.
[6] Wang L, Fu S, Liang J, Shang J, Wang J. A review on gas hydrate developments propped by worldwide national projects. Geol China 2017;44:439–48.
[7] Dudley B. BP energy outlook. London, UK: BP Energy Economics; 2018.
[8] Wang Y-F, Wang L-B, Li Y, Gu J-X, Sun C-Y, Chen G-J, et al. Effect of temperature on gas production from hydrate-bearing sediments by using a large 196-L reactor. Fuel 2020;275:117963.
[9] Yang M, Fu Z, Jiang L, Song Y. Gas recovery from depressurized methane hydrate deposits with different water saturations. Appl Energy 2017;187:180–8.
[10] Tupsakhare SS, Kattekola S, Castaldi MJ. An Application of the Results from the Large-Scale Thermal Stimulation Method of Methane Hydrate Dissociation to the Field Tests. Ind Eng Chem Res 2017;56:4588–99. https://doi.org/10.1021/acs.iecr.7b00553.
[11] Li B, Liu SD, Liang YP, Liu H. The use of electrical heating for the enhancement of gas recovery from methane hydrate in porous media. Appl Energy 2018;227:694–702. https://doi.org/10.1016/j.apenergy.2017.08.066.
[12] Yuan Q, Sun C-Y, Wang X-H, Zeng X-Y, Yang X, Liu B, et al. Experimental study of gas production from hydrate dissociation with continuous injection mode using a three-dimensional quiescent reactor. Fuel 2013;106:417–24.
[13] Li G, Wu DM, Sen LX, Zhang Y, Lv QN, Wang Y. Experimental Investigation into the Production Behavior of Methane Hydrate under Methanol Injection in Quartz Sand. Energy Fuels 2017;31:5411–8. https://doi.org/10.1021/acs.energyfuels.7b00464.
[14] Mu L, von Solms N. Methane Production and Carbon Capture by Hydrate Swapping. Energy Fuels 2016;31:3338–47. https://doi.org/10.1021/acs.energyfuels.6b01638.
[15] Xu C-G, Cai J, Yu Y-S, Chen Z-Y, Li X-S. Research on micro-mechanism and efficiency of CH4 exploitation via CH4-CO2 replacement from natural gas hydrates. Fuel 2018;216:255–65. https://doi.org/10.1016/j.fuel.2017.12.022.
[16] Koh D-Y, Kang H, Lee J-W, Park Y, Kim S-J, Lee J, et al. Energy-efficient natural gas hydrate production using gas exchange. Appl Energy 2016;162:114–30.
[17] Merey S, Al-Raoush RI, Jung J, Alshibli KA. Comprehensive literature review on CH4-CO2 replacement in microscale porous media. J Pet Sci Eng 2018;171:48–62. https://doi.org/10.1016/j.petrol.2018.07.032.
[18] Ersland G, Husebø J, Graue A, Baldwin BA, Howard J, Stevens J. Measuring gas hydrate formation and exchange with CO2 in Bentheim sandstone using MRI tomography. Chem Eng J 2010;158:25–31. https://doi.org/10.1016/j.cej.2008.12.028.
[19] Wu G, Tian L, Chen D, Niu M, Ji H. CO2 and CH4 Hydrates: Replacement or Cogrowth? J Phys Chem C 2019;123(22):13401–9.
[20] Sun J, Ning F, Zhang L, Liu T, Peng Li, Liu Z, et al. Numerical simulation on gas production from hydrate reservoir at the 1st offshore test site in the eastern Nankai Trough. J Nat Gas Sci Eng 2016;30:64–76.
[21] Li J, Ye J, Qin X, Qiu H, Wu N, Lu H, et al. The first offshore natural gas hydrate production test in South China Sea. China Geol 2018;1:5–16. https://doi.org/10.31035/cg2018003.
[22] Moridis GJ, Collett TS, Dallimore SR, Satoh T, Hancock S, Weatherill B. Numerical studies of gas production from several CH4 hydrate zones at the Mallik site, Mackenzie Delta. Canada J Pet Sci Eng 2004;43:219–38. https://doi.org/10.1016/j.petrol.2004.02.015.
[23] Yamamoto K, Dallimore S. Aurora-JOGMEC-NRCan Mallik 2006–2008 gas hydrate research project progress. Nat Gas Oil 2008;304:285–4541.
[24] Nair VC, Prasad SK, Kumar R, Sangwai JS. Energy recovery from simulated clayey gas hydrate reservoir using depressurization by constant rate gas release, thermal stimulation and their combinations. Appl Energy 2018;225:755–68. https://doi.org/10.1016/j.apenergy.2018.05.028.
[25] Chandrasekharan Nair V, Gupta P, Sangwai JS. Natural Gas Production from a Marine Clayey Hydrate Reservoir Formed in Seawater Using Depressurization at Constant Pressure, Depressurization by Constant Rate Gas Release, Thermal Stimulation, and Their Implications for Real Field Applications. Energy Fuels 2019;33:3108–22. https://doi.org/10.1021/acs.energyfuels.9b00187.
[26] Konno Y, Masuda Y, Akamine K, Naiki M, Nagao J. Sustainable gas production from methane hydrate reservoirs by the cyclic depressurization method. Energy Convers Manag 2016;108:439–45.
[27] Wang Y, Feng JC, Sen LX, Zhan L, Li XY. Pilot-scale experimental evaluation of gas recovery from methane hydrate using cycling-depressurization scheme. Energy 2018;160:835–44. https://doi.org/10.1016/j.energy.2018.07.054.
[28] Zhao J, Liu Y, Guo X, Wei R, Yu T, Xu L, et al. Gas production behavior from hydrate-bearing fine natural sediments through optimized step-wise depressurization. Appl Energy 2020;260:114275.
[29] Guo X, Xu L, Wang B, Sun L, Liu Y, Wei R, et al. Optimized gas and water production from water-saturated hydrate-bearing sediment through step-wise depressurization combined with thermal stimulation. Appl Energy 2020;276:115438.
[30] Phillips SC, Flemings PB, You K, Meyer DW, Dong T. Investigation of in situ salinity and methane hydrate dissociation in coarse-grained sediments by slow, stepwise depressurization. Mar Pet Geol 2019;109:128–44.
[31] Sun L, Wang T, Dong Bo, Li M, Yang L, Dong H, et al. Pressure oscillation controlled CH4/CO2 replacement in methane hydrates: CH4 recovery, CO2 storage, and their characteristics. Chem Eng J 2021;425:129709.
[32] Wang Y, Lang X, Fan S, Wang S, Yu C, Li G. Review on Enhanced Technology of Natural Gas Hydrate Recovery by Carbon Dioxide Replacement. Energy Fuels 2021;35:3659–74. https://doi.org/10.1021/acs.energyfuels.0c04138.
[33] Pandey JS, von Solms N. Hydrate Stability and Methane Recovery from Gas Hydrate through CH4–CO2 Replacement in Different Mass Transfer Scenarios. Energies 2019;12:2309. https://doi.org/10.3390/en12122309.

[34] Liang H, Guan D, Shi K, Yang L, Zhang L, Zhao J, et al. Characterizing Mass-Transfer mechanism during gas hydrate formation from water droplets. Chem Eng J 2022;428:132626.
[35] Liang H, Yang L, Song Y, Zhao J. New Approach for Determining the Reaction Rate Constant of Hydrate Formation via X-ray Computed Tomography. J Phys Chem C 2021;125:42–8. https://doi.org/10.1021/acs.jpcc.0c07801.
[36] Zhao J, Zhang L, Chen X, Zhang Y, Liu Y, Song Y. Combined replacement and depressurization methane hydrate recovery method. Energy Explor Exploit 2016; 34:129–39. https://doi.org/10.1177/0144598715623676.
[37] Pandey JS, Karantonidis C, Karcz AP, von Solms N. Enhanced CH4-CO2 Hydrate Swapping in the Presence of Low Dosage Methanol. Energies 2020;13:5238. https://doi.org/10.3390/en13205238.
[38] Ouyang Q, Fan S, Wang Y, Lang X, Wang S, Zhang Y, et al. Enhanced Methane Production Efficiency with in Situ Intermittent Heating Assisted CO2Replacement of Hydrates. Energy Fuels 2020;34(10):12476–85.
[39] Boswell R, Schoderbek D, Collett TS, Ohtsuki S, White M, Anderson BJ. The Iḡnik Sikumi Field Experiment, Alaska North Slope: Design, Operations, and Implications for CO2–CH4 Exchange in Gas Hydrate Reservoirs. Energy Fuels 2016;31:140–53. https://doi.org/10.1021/acs.energyfuels.6b01909.
[40] Chen Y, Gao YH, Chen LT, Wang XR, Liu K, Sun BJ. Experimental investigation of the behavior of methane gas hydrates during depressurization-assisted CO2 replacement. J Nat Gas Sci Eng 2019;61:284–92. https://doi.org/10.1016/j.jngse.2018.11.015.
[41] Yang J, Okwananke A, Tohidi B, Chuvilin E, Maerle K, Istomin V, et al. Flue gas injection into gas hydrate reservoirs for methane recovery and carbon dioxide sequestration. Energy Convers Manag 2017;136:431–8.
[42] Hassanpouryouzband A, Yang J, Okwananke A, Burgass R, Tohidi B, Chuvilin E, et al. An Experimental Investigation on the Kinetics of Integrated Methane Recovery and CO2 Sequestration by Injection of Flue Gas into Permafrost Methane Hydrate Reservoirs. Sci Rep 2019;9(1). https://doi.org/10.1038/s41598-019-52745-x.
[43] Heydari A, Peyvandi K. Study of biosurfactant effects on methane recovery from gas hydrate by CO2 replacement and depressurization. Fuel 2020;272:117681. https://doi.org/10.1016/j.fuel.2020.117681.
[44] Goel N. In situ methane hydrate dissociation with carbon dioxide sequestration: Current knowledge and issues. J Pet Sci Eng 2006;51:169–84. https://doi.org/10.1016/j.petrol.2006.01.005.
[45] Pandey JS, Ouyang Q, von Solms N. New insights into the dissociation of mixed CH4/CO2 hydrates for CH4 production and CO2 storage. Chem Eng J 2022;427: 131915. https://doi.org/10.1016/j.cej.2021.131915.
[46] Pandey JS, Strand Ø, von Solms N, Ersland G, Almenningen S. Direct Visualization of CH4/CO2 Hydrate Phase Transitions in Sandstone Pores. Cryst Growth Des 2021;21:2793–806. https://doi.org/10.1021/acs.cgd.0c01714.
[47] Liu W, Luo T, Li Y, Song Y, Zhu Y, Liu Yu, et al. Experimental study on the mechanical properties of sediments containing CH 4 and CO 2 hydrate mixtures. J Nat Gas Sci Eng 2016;32:20–7.
[48] Wu P, Li Y, Sun X, Liu W, Song Y. Mechanical Characteristics of Hydrate-Bearing Sediment: A Review. Energy Fuels 2021;35:1041–57. https://doi.org/10.1021/acs.energyfuels.0c03995.
[49] Zhou X, Fan S, Liang D, Wang D, Huang N. Use of Electrical Resistance to Detect the Formation and Decomposition of Methane Hydrate. J Nat Gas Chem 2007;16: 399–403. https://doi.org/10.1016/S1003-9953(08)60011-0.
[50] Li F-G, Sun C-Y, Li S-L, Chen G-J, Guo X-Q, Yang L-Y, et al. Experimental Studies on the Evolvement of Electrical Resistivity during Methane Hydrate Formation in Sediments. Energy Fuels 2012;26(10):6210–7.
[51] Ren SR, Liu Y, Liu Y, Zhang W. Acoustic velocity and electrical resistance of hydrate bearing sediments. J Pet Sci Eng 2010;70:52–6. https://doi.org/10.1016/j.petrol.2009.09.001.
[52] Stern LA, Constable S, Lu R, Du Frane WL, Roberts JM. Electrical conductivity of pure CO2 hydrate and CH4 hydrate: Role of the guest molecule 2021.
[53] Shi M, Woodley JM, von Solms N. An Experimental Study on Improved Production Performance by Depressurization Combined with CO2-Enriched Air Injection. Energy Fuels 2020;34:7329–39. https://doi.org/10.1021/acs.energyfuels.0c00779.
[54] Pandey JS, Karantonidis C, Ouyang Q, von Solms N. Cyclic Depressurization-Driven Enhanced CH4 Recovery after CH4–CO2 Hydrate Swapping. Energy Fuels 2021;35:9521–37. https://doi.org/10.1021/acs.energyfuels.1c00685.
[55] Pandey JS, Khan S, Karcz AP, von Solms N. Chemically modified hydrate swapping and hydrate stability during multistage CO2-N2 injection schemes. Fuel 2021;299: 120711. https://doi.org/10.1016/j.fuel.2021.120711.
[56] Le TX, Rodts S, Hautemayou D, Aimedieu P, Bornert M, Chabot B, et al. Kinetics of methane hydrate formation and dissociation in sand sediment. Geomech Energy Environ 2020;23:100103. https://doi.org/10.1016/j.gete.2018.09.007.
[57] Wu R, Kozielski KA, Hartley PG, May EF, Boxall J, Maeda N. Probability distributions of gas hydrate formation. AIChE J 2013;59(7):2640–6.
[58] Kumar A, Maini B, Bishnoi PR, Clarke M, Zatsepina O, Srinivasan S. Experimental determination of permeability in the presence of hydrates and its effect on the dissociation characteristics of gas hydrates in porous media. J Pet Sci Eng 2010;70: 114–22. https://doi.org/10.1016/j.petrol.2009.10.005.
[59] Davies SR, Sloan ED, Sum AK, Koh CA. In Situ Studies of the Mass Transfer Mechanism across a Methane Hydrate Film Using High-Resolution Confocal Raman Spectroscopy. J Phys Chem C 2010;114:1173–80. https://doi.org/10.1021/jp909416y.
[60] Salamatin AN, Falenty A, Kuhs WF. Diffusion Model for Gas Replacement in an Isostructural CH4-CO2 Hydrate System. J Phys Chem C 2017;121(33):17603–16.
[61] Waage MH, Trinh TT, van Erp TS. Diffusion of gas mixtures in the sI hydrate structure. J Chem Phys 2018;148(21):214701.
[62] CSM. Colorado School of Mines Hydrate Software 2015 n.d. http://hydrates.mines.edu/CHR/Software.html.
[63] Jadhawar P, Yang J, Chapoy A, Tohidi B. Subsurface Carbon Dioxide Sequestration and Storage in Methane Hydrate Reservoirs Combined with Clean Methane Energy Recovery. Energy Fuels 2020;35:1567–79. https://doi.org/10.1021/acs.energyfuels.0c02839.
[64] Fan S, Wang X, Lang X, Wang Y. Energy efficiency simulation of the process of gas hydrate exploitation from flue gas in an electric power plant. Nat Gas Ind B 2017;4: 470–6. https://doi.org/https://doi.org/10.1016/j.ngib.2017.09.009.
[65] Kong Z, Jiang Q, Dong X, Wang J, Wan X. Estimation of China's production efficiency of natural gas hydrates in the South China Sea. J Clean Prod 2018;203: 1–12. https://doi.org/10.1016/j.jclepro.2018.08.262.
[66] Li X-Y, Li X-S, Wang Y, Liu J-W, Hu H-Q. The determining factor of hydrate dissociation rate in the sediments with different water saturations. Energy 2020; 202:117690. https://doi.org/10.1016/j.energy.2020.117690.
[67] Sun Y-F, Zhong J-R, Chen G-J, Cao B-J, Li R, Chen D-Y. A new approach to efficient and safe gas production from unsealed marine hydrate deposits. Appl Energy 2021; 282:116259. https://doi.org/10.1016/j.apenergy.2020.116259.
[68] He J, Li X, Chen Z, You C, Peng H, Zhang Z. Sustainable hydrate production using intermittent depressurization in hydrate-bearing reservoirs connected with water layers. Energy 2022;238:121752. https://doi.org/10.1016/j.energy.2021.121752.